Nanosized Layered TOT Magnesium-Silicates: Equilibrium Morphologies and Surface Speciation, a Computational and Experimental Study

Hervé Toulhoat, Longfei Lin †, Dalil Brouri, Jean-Marc Krafft, Yannick Millot, Guillaume Laugel, Hélène Lauron-Pernot*

Sorbonne Université, CNRS, Laboratoire de Réactivité de Surface, F-75005, Paris, France

Supporting Information.

AUTHOR INFORMATION

Corresponding Author

* herve.toulhoat@orange.fr

Present Addresses

† Present address: School of Chemistry, University of Manchester, Oxford Road, Manchester, M13 9PL, UK.

1 Correlations between computed shielding constants and experimental chemical shifts for ^{29}Si, ^{25}Mg, and ^{1}H NMR

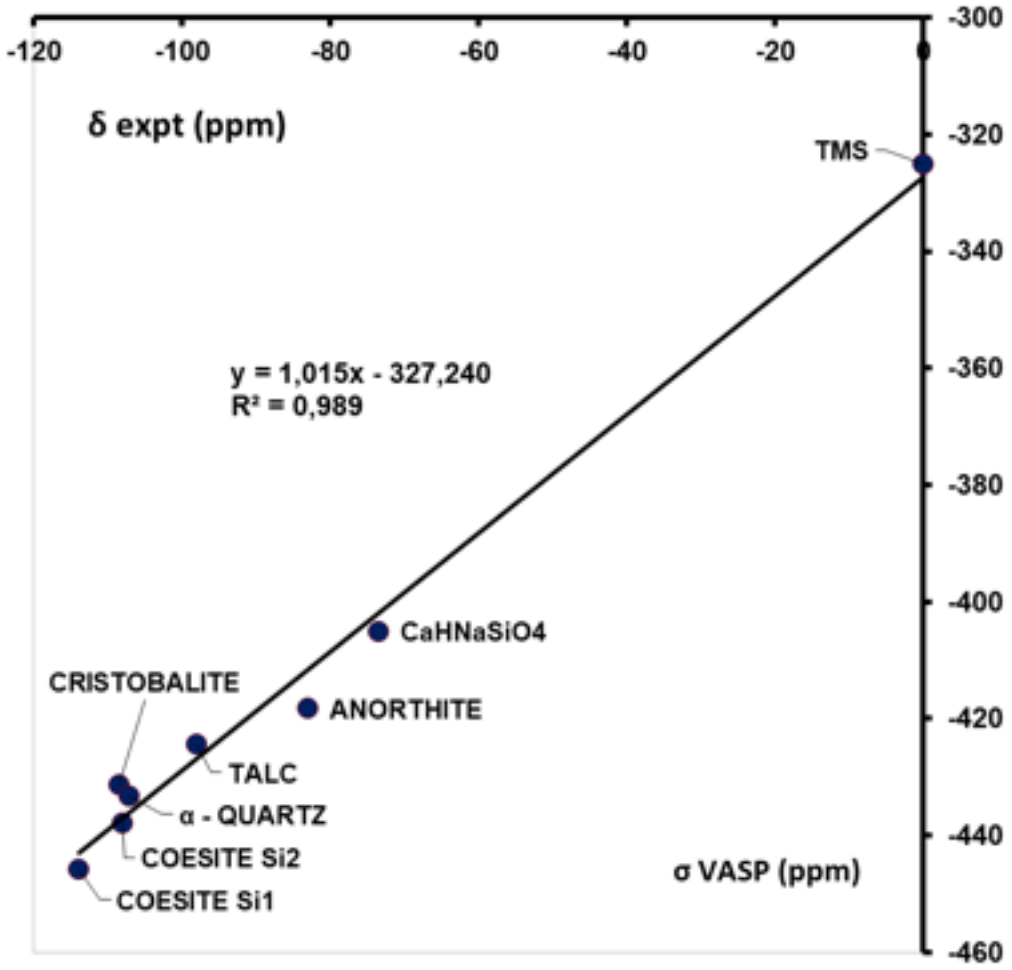

Figure S1: Correlation obtained between computed shielding constant σ and experimental chemical shift δ for ^{29}Si NMR (reference TMS)

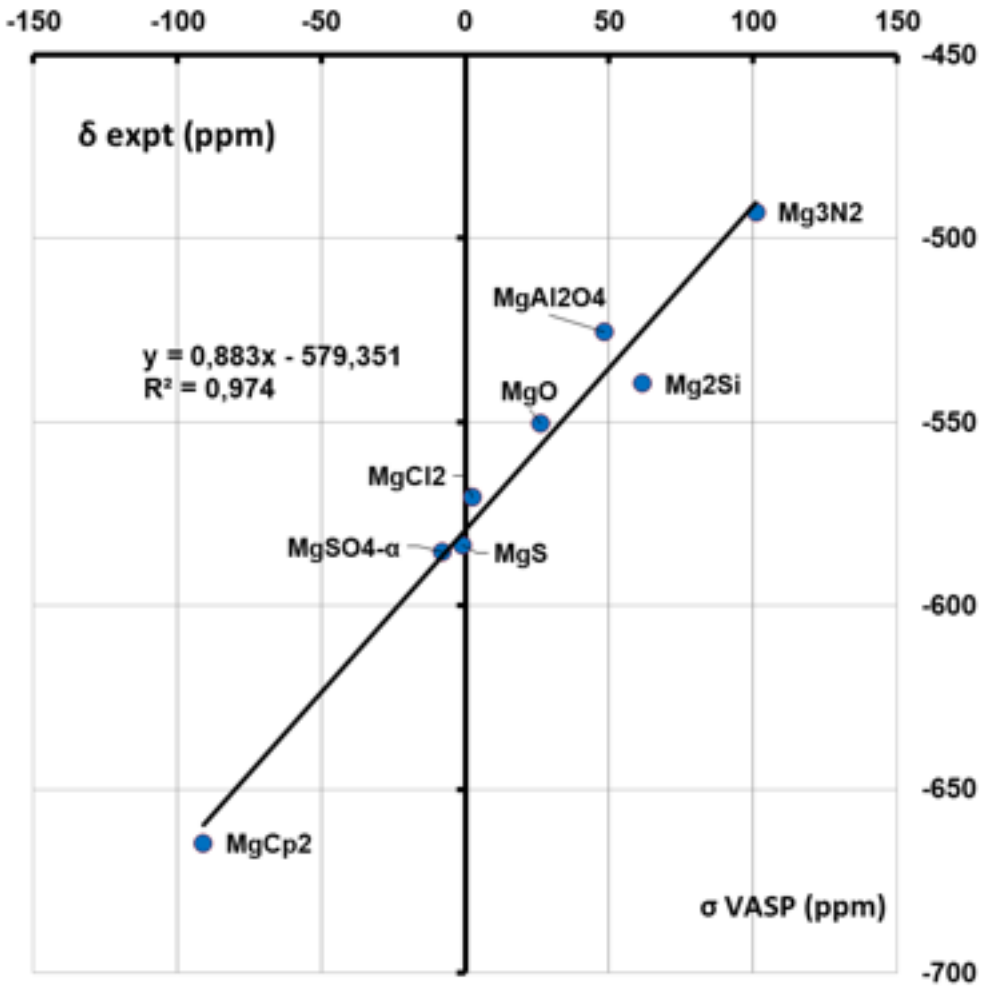

Figure S2: Correlation obtained between computed shielding constant σ and experimental chemical shift δ for ^{25}Mg NMR (reference aqueous $MgCl_2$ 1M)

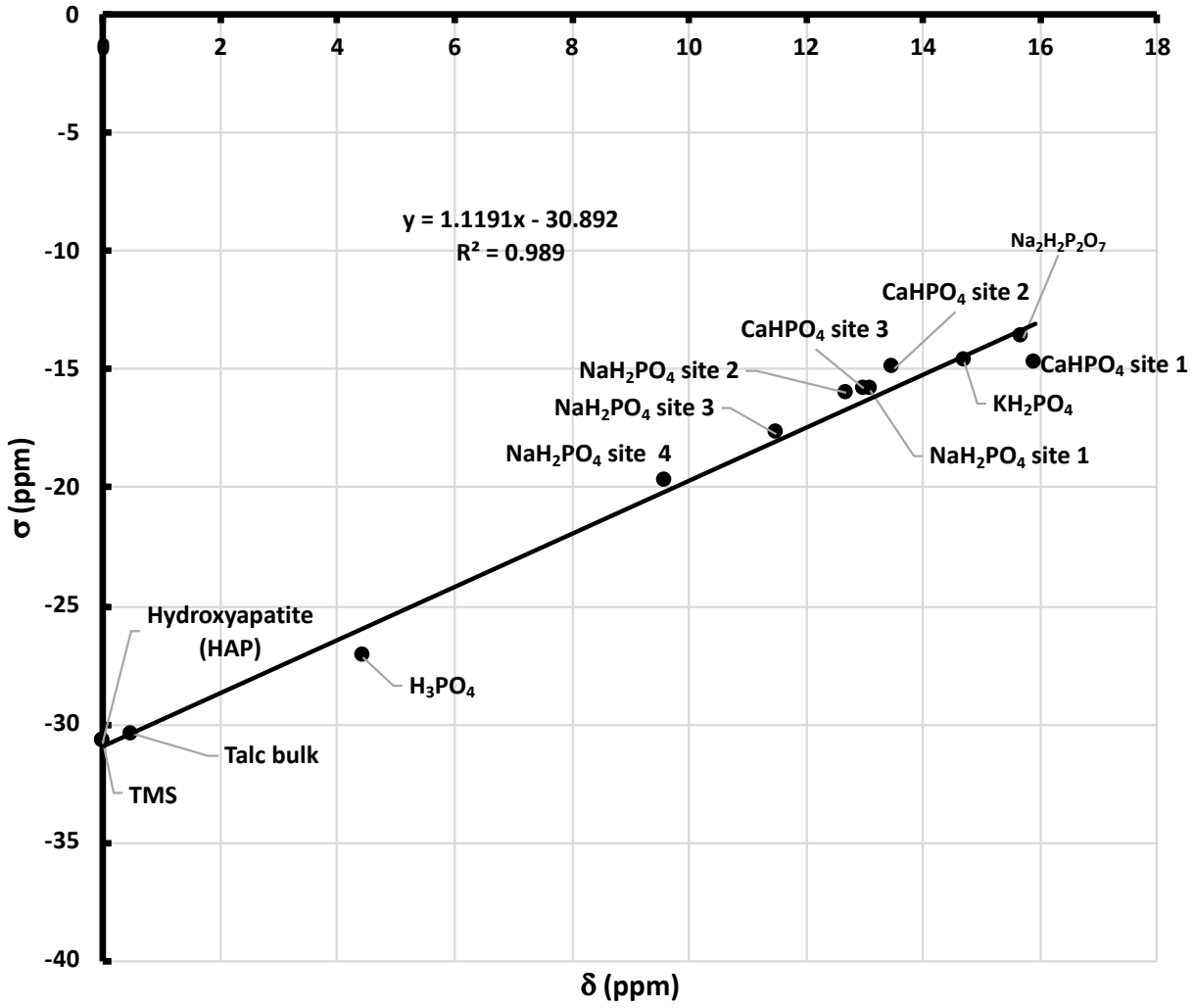

Figure S3: Correlation obtained between computed shielding constant σ and experimental chemical shift δ for ^{1}H NMR (reference TMS)

2 Calculated normal modes of vibration obtained for the {130}, {100} slab models of Talc edges at zero, low and high coverage by water (corrected for anharmonicity)

Table S1: Calculated higher normal modes of vibration in cm^{-1}, obtained the {130}, {100} slab models of Talc edges at high (HC), low (LC) and zero (0W) coverage by water (corrected for anharmonicity). Simulations of P1 bulk Talc provide for reference a range of Mg-**OH** stretching modes. Colour code for assignments: orange, Mg_{surf}-**OH** stretching; red, Si_{surf}-**OH** stretching, brown, coupled Mg_{surf}-**OH** and Si_{surf}-**OH** stretching; yellow, Mg_{bulk}-**OH** stretching; green, Mg_{surf}-H**OH** stretching; blue, Mg_{surf}-**HOH** bending

{130} HC	{130} LC	{130} 0W	{100} HC	{100} LC	{100} 0W	Talc bulk
4048.7	3736.0	3766.7	3735.1	3748.2	3784.0	3754.5
3988.0	3735.9	3766.7	3727.5	3740.6	3783.8	3749.8
3803.3	3735.1	3766.1	3725.9	3692.5	3463.4	3662.9
3732.9	3733.8	3764.8	3721.4	3689.5	3462.8	3661.7
3732.3	3733.6	3724.2	3720.2	3688.3	3064.1	3654.7
3730.7	3733.2	3723.8	3718.3	3686.0	3053.3	3645.7
3730.5	3732.3	3723.4	3714.7	3681.7		3644.5
3729.5	3732.1	3721.3	3712.2	3680.0		3640.9
3728.1	3729.5		3710.7	3676.0		
3727.1	3729.4		3709.0	3674.4		
3726.6	3728.5		3707.8	3650.3		
3725.7	3728.4		3698.7	3649.2		
3724.2	3727.1		3697.1	3633.0		
3723.8	3726.7		3694.8	3631.7		
3722.6	3684.2		3670.8			
3721.8	3683.9		3630.6			
3721.6	3683.5		3584.5			
3720.6	3683.4		3530.8			
3718.9	3676.2		3441.7			
3677.0	3675.5		3404.3			
3676.7	3641.9		3380.5			
3716.4	3640.6		3307.4			
3715.1	3640.1		3298.8			

3681.3	3640.0		3247.9		
3663.7			3194.1		
{130} HC	{130} LC	{130} 0W	{100} HC	{100} LC	{100} 0W	Talc bulk
3661.6			3150.8		
3655.0			1626.1		
3650.5			1623.4		
3602.6			1601.4		
3601.2			1596.4		
3581.6			1591.4		
3581.1			1551.6		
3486.6					
3462.0					
3444.6					
3442.6					
3420.7					
3415.0					
3406.7					
3339.2					
3271.5					
3231.0					
3210.7					
3201.8					
3190.0					
3070.4					
3068.9					
3061.7					
1643.1					
1637.7					
1636.6					
1629.8					
1615.8					
1606.8					
1604.6					
1602.8					
1601.8					
1597.2					
1592.1					
1588.5					

3 Geometry optimized conformations of CO adsorbed on Talc edges slab models

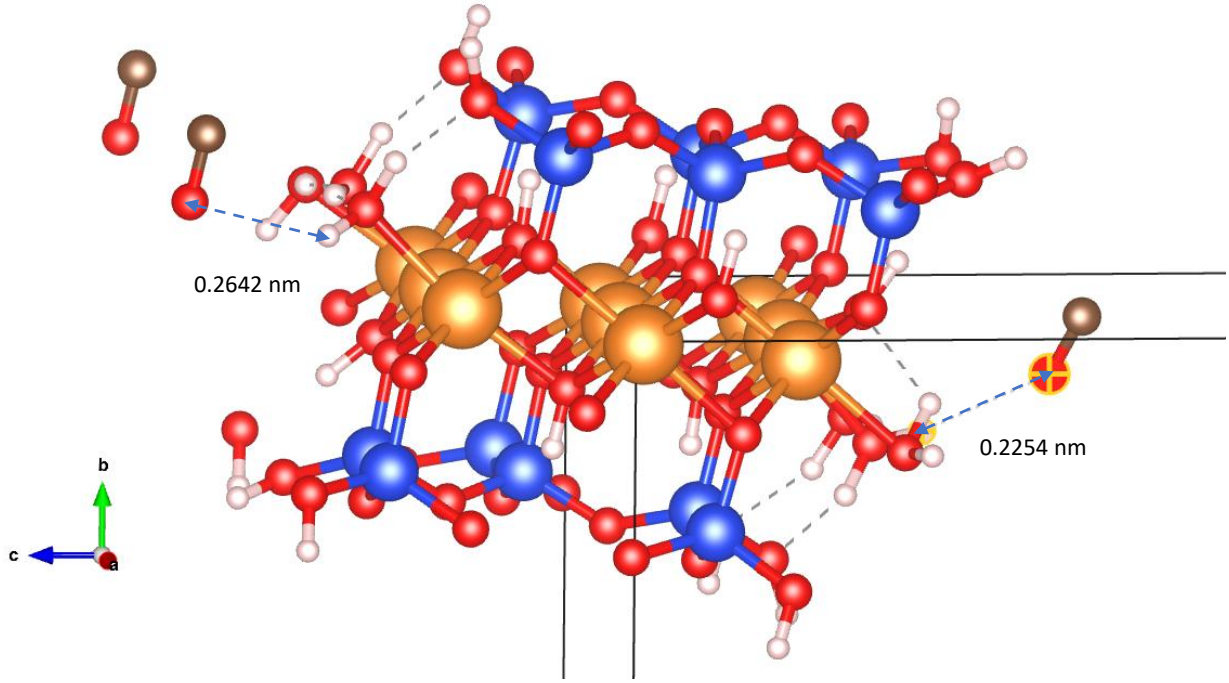

Figure S4 {100} HC_CO_A

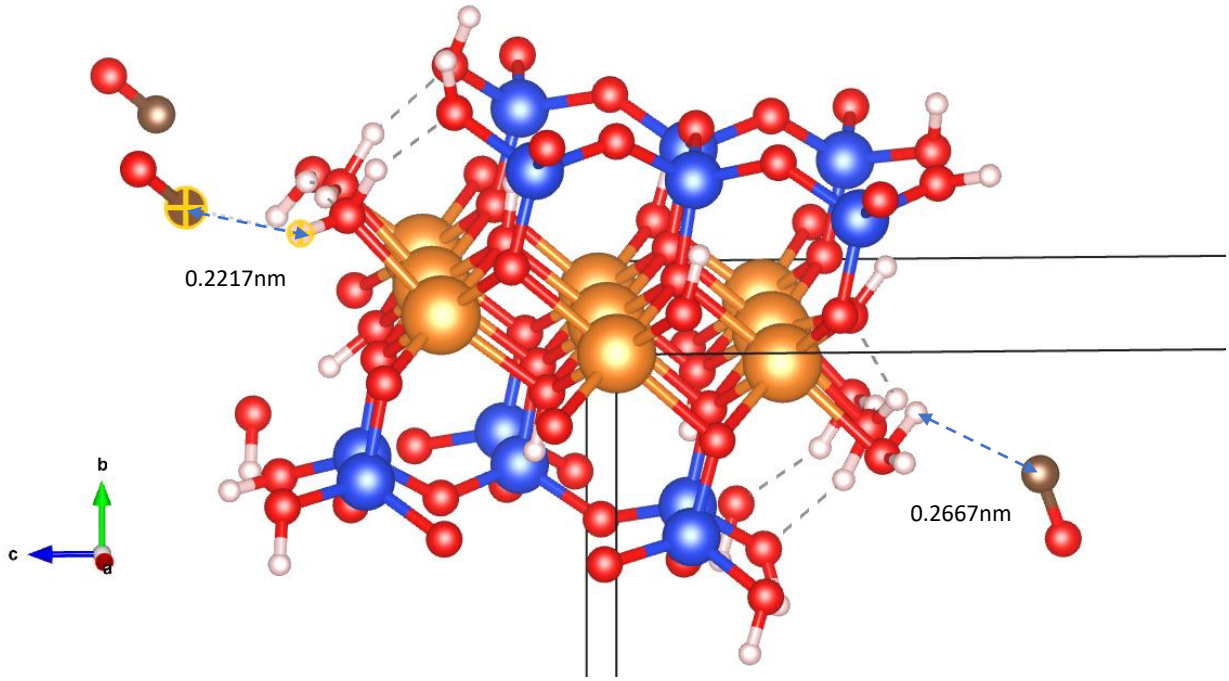

Figure S5 {100} HC_OC_A

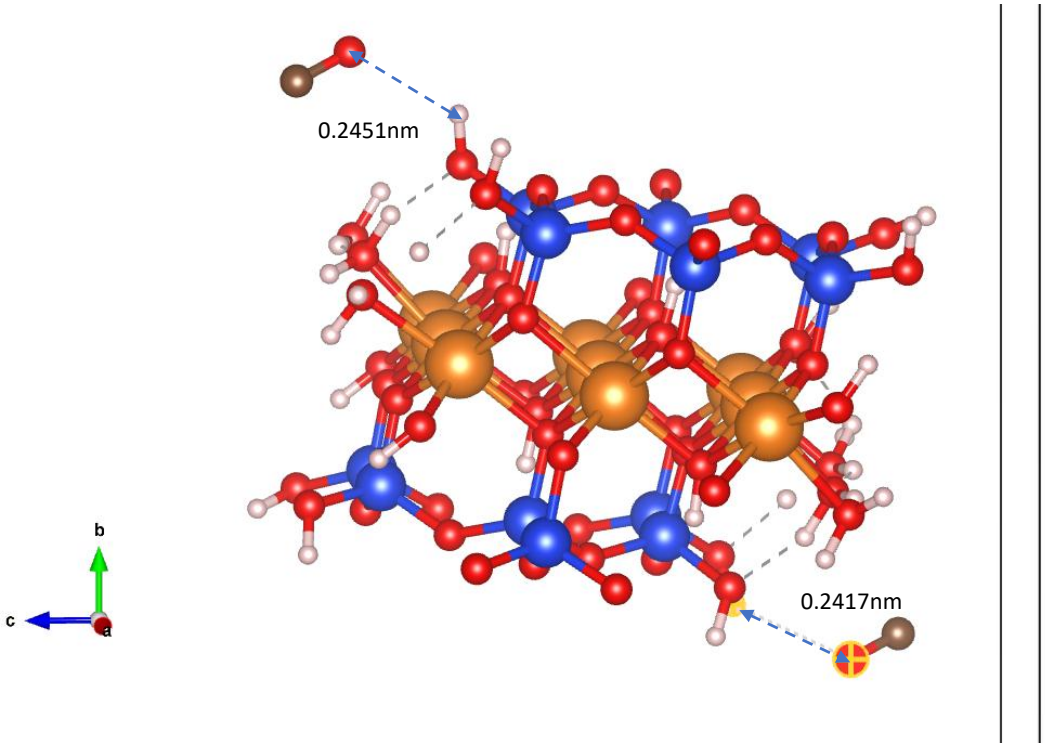

Figure S6 {100} HC_CO_B

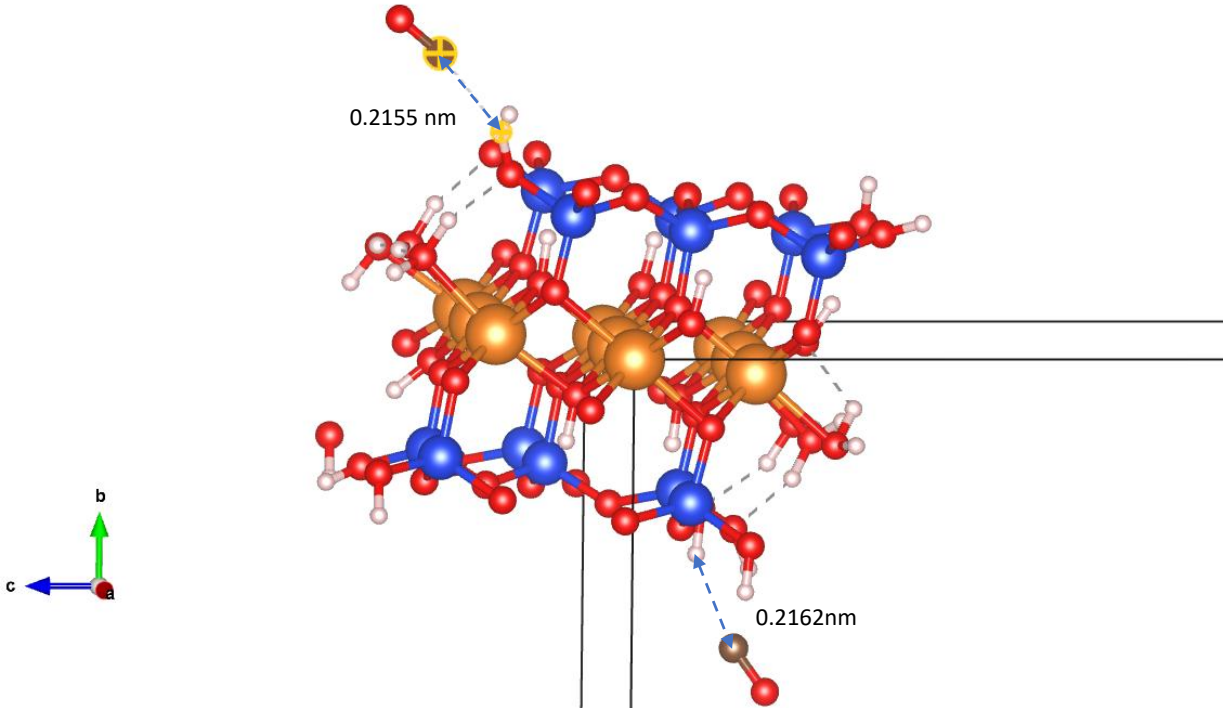

Figure S7 {100} HC_OC_B

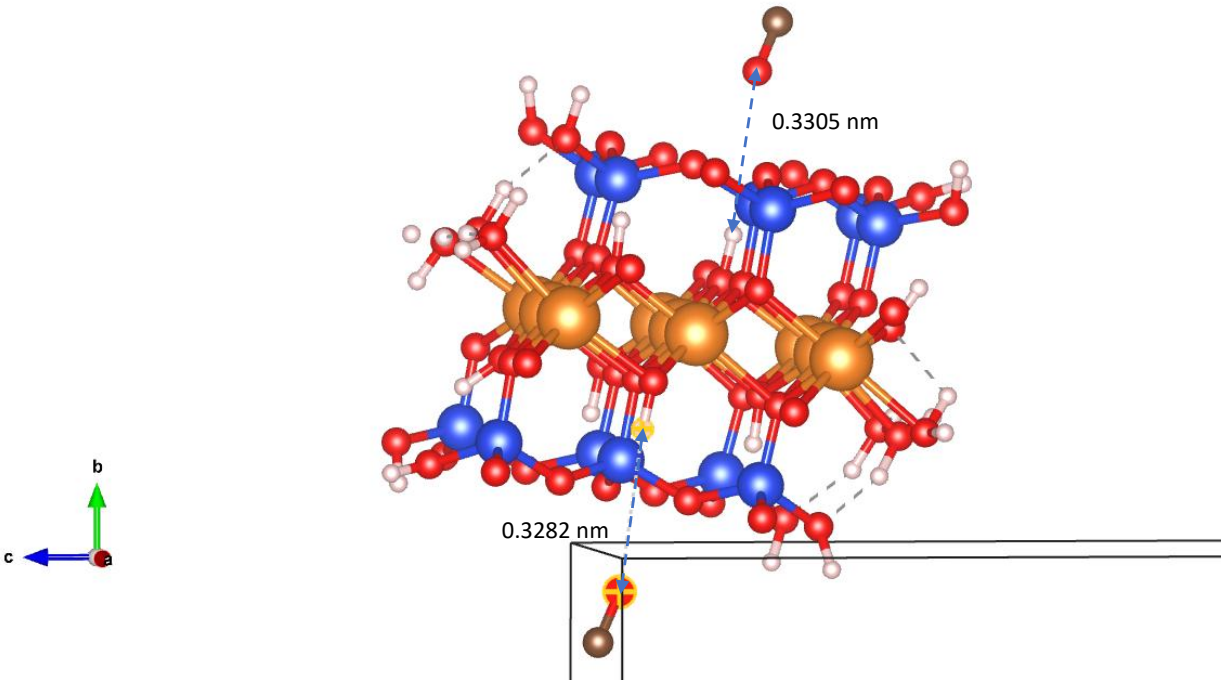

Figure S8 {100} HC_CO_C

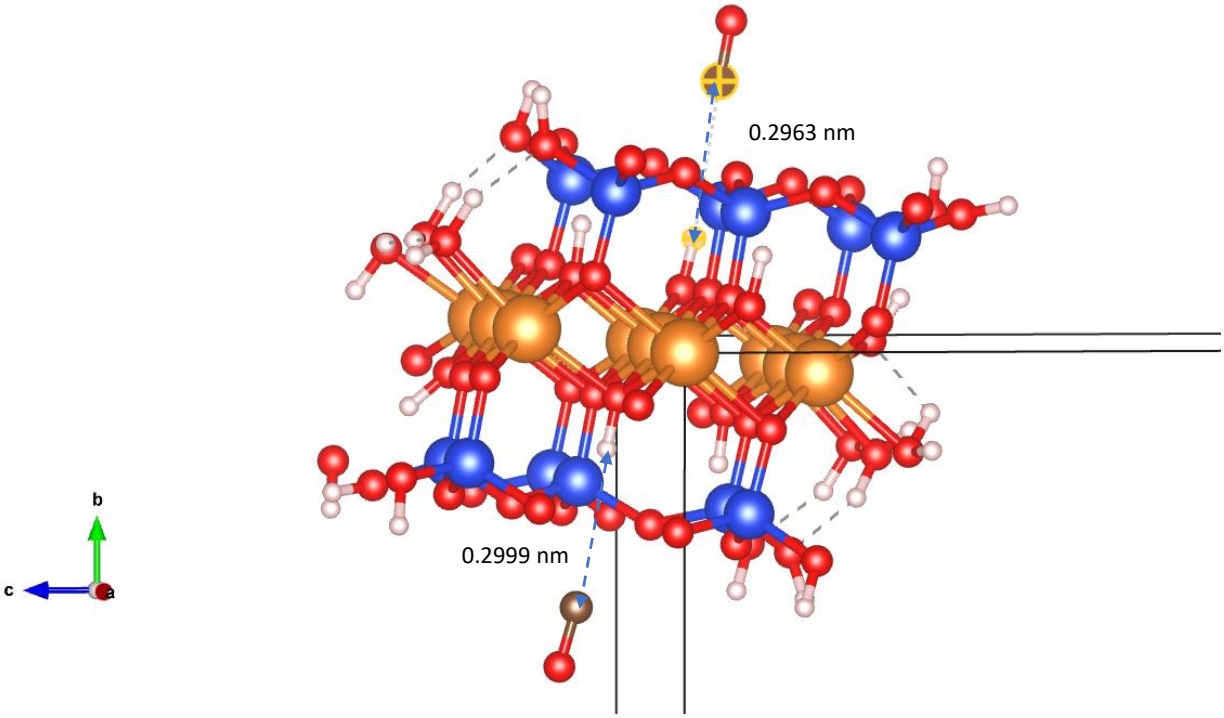

Figure S9 {100} HC_OC_C

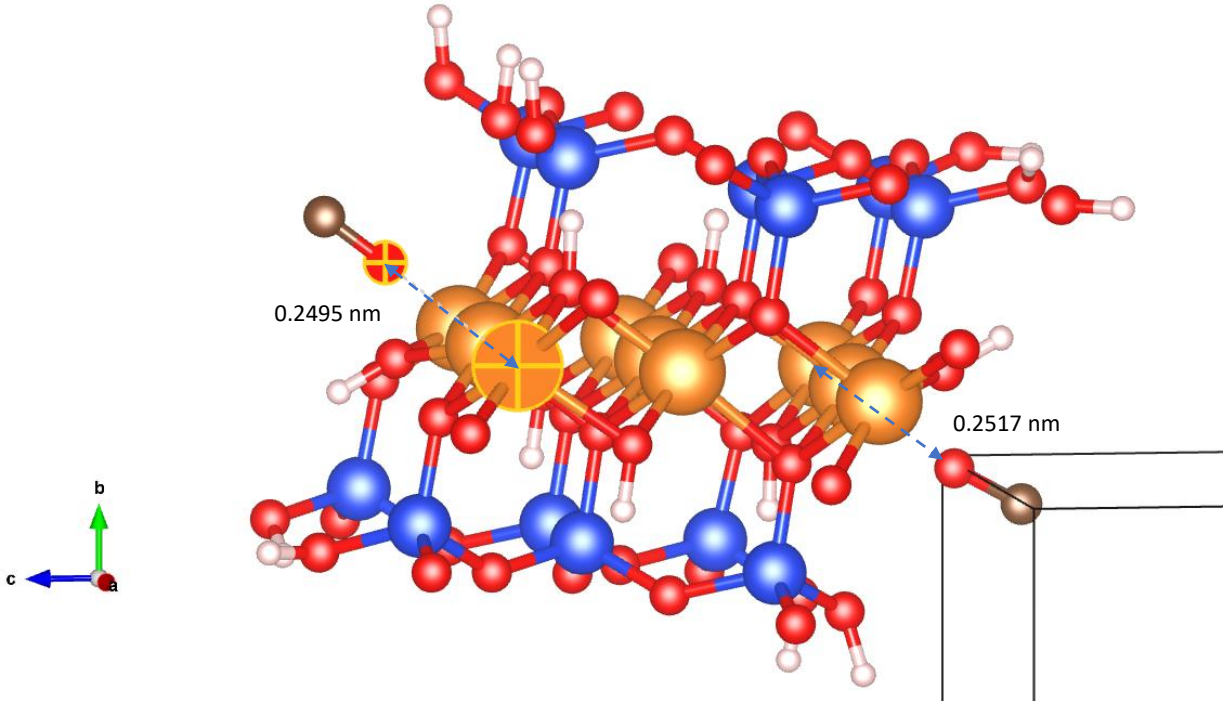

Figure S10 {100} LC_CO_A

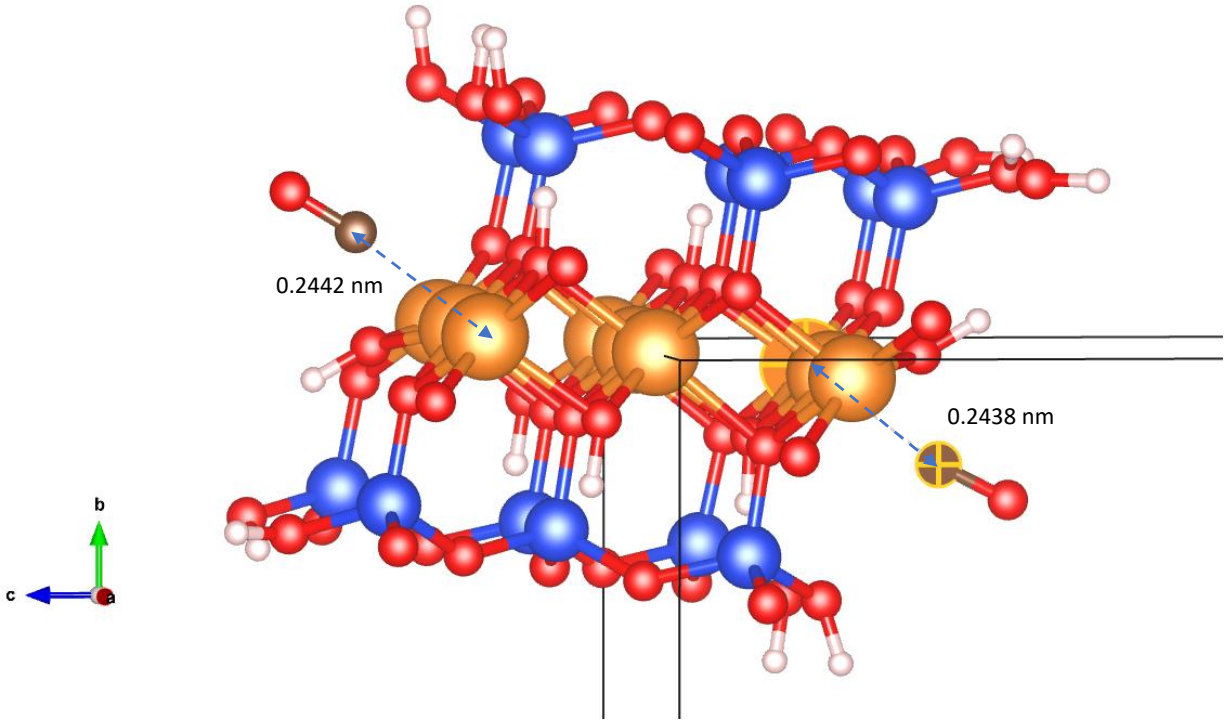

Figure S11 {100} LC_OC_A

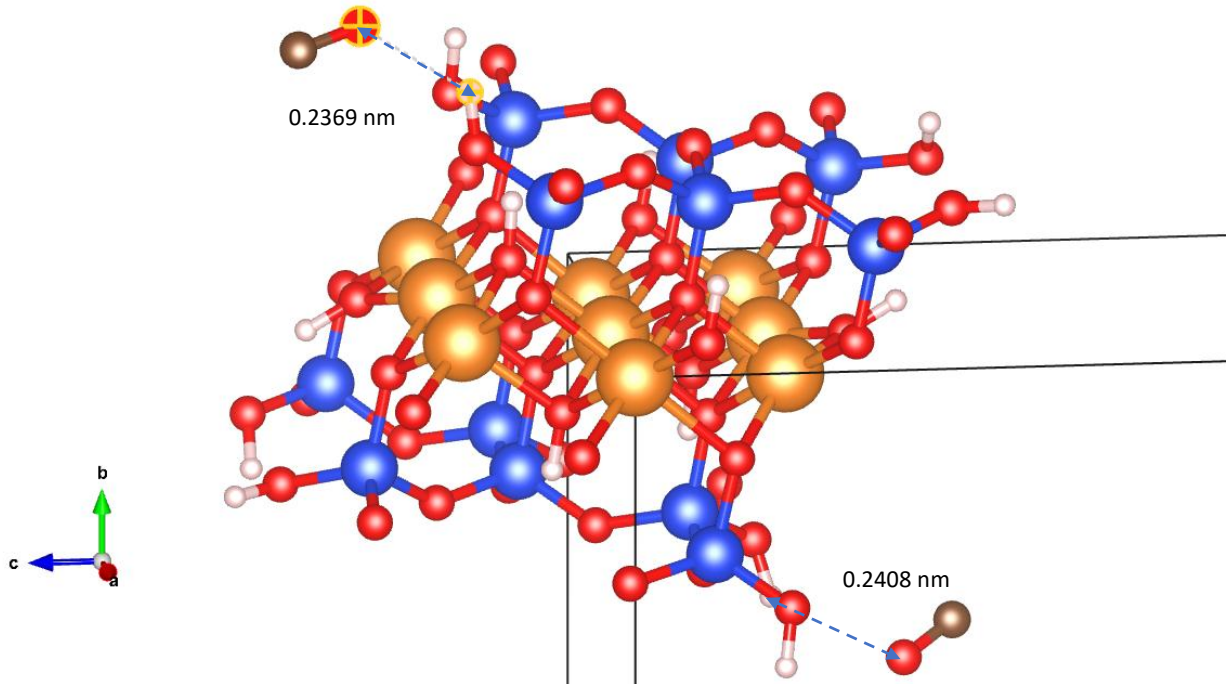

Figure S12 {100} LC_CO_B

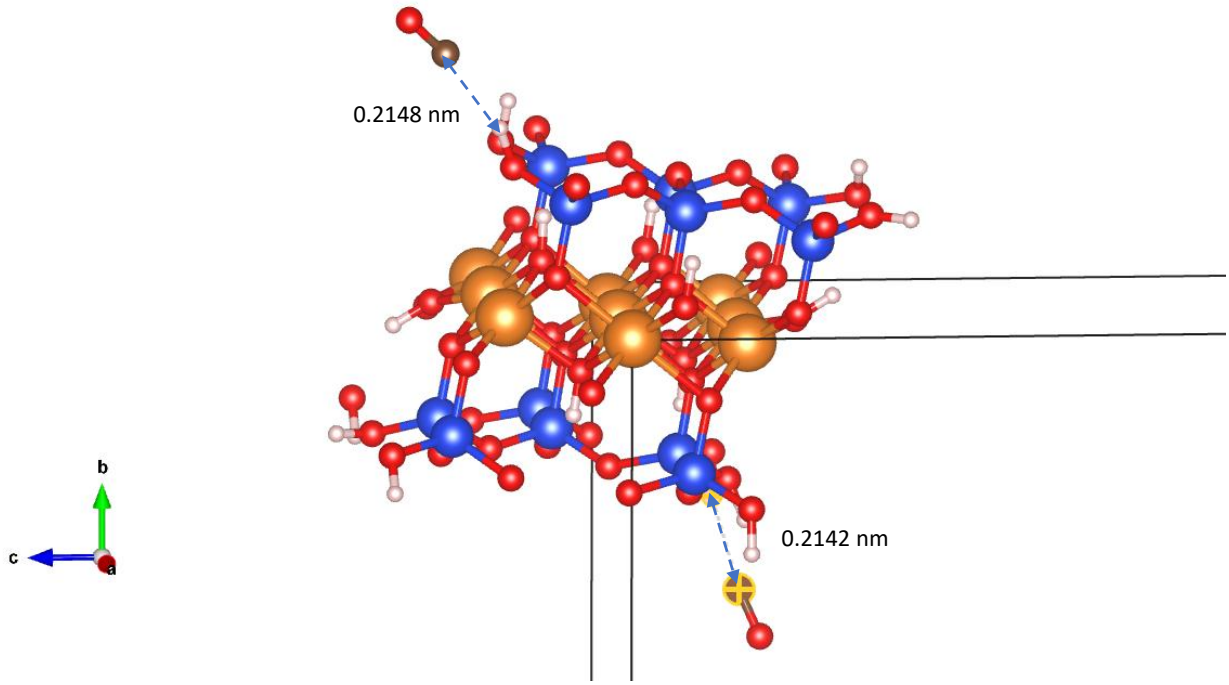

Figure S13 {100} LC_OC_B

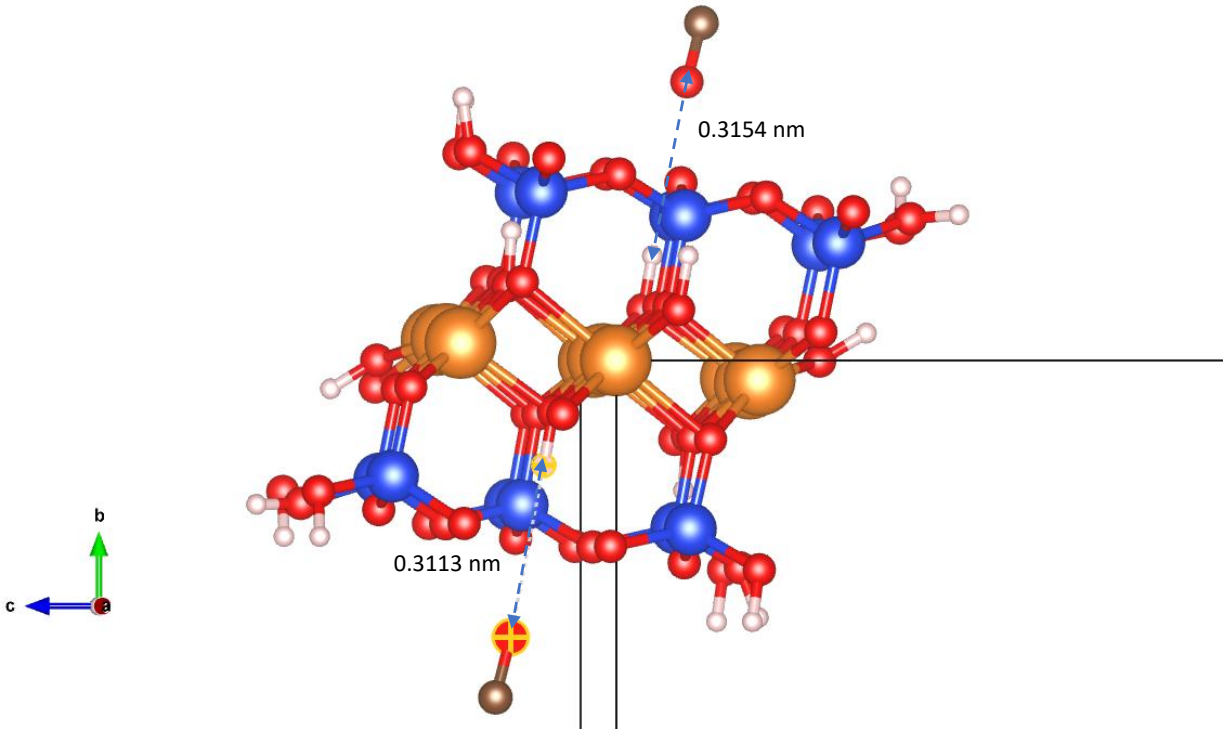

Figure S14 {100} LC_CO_C

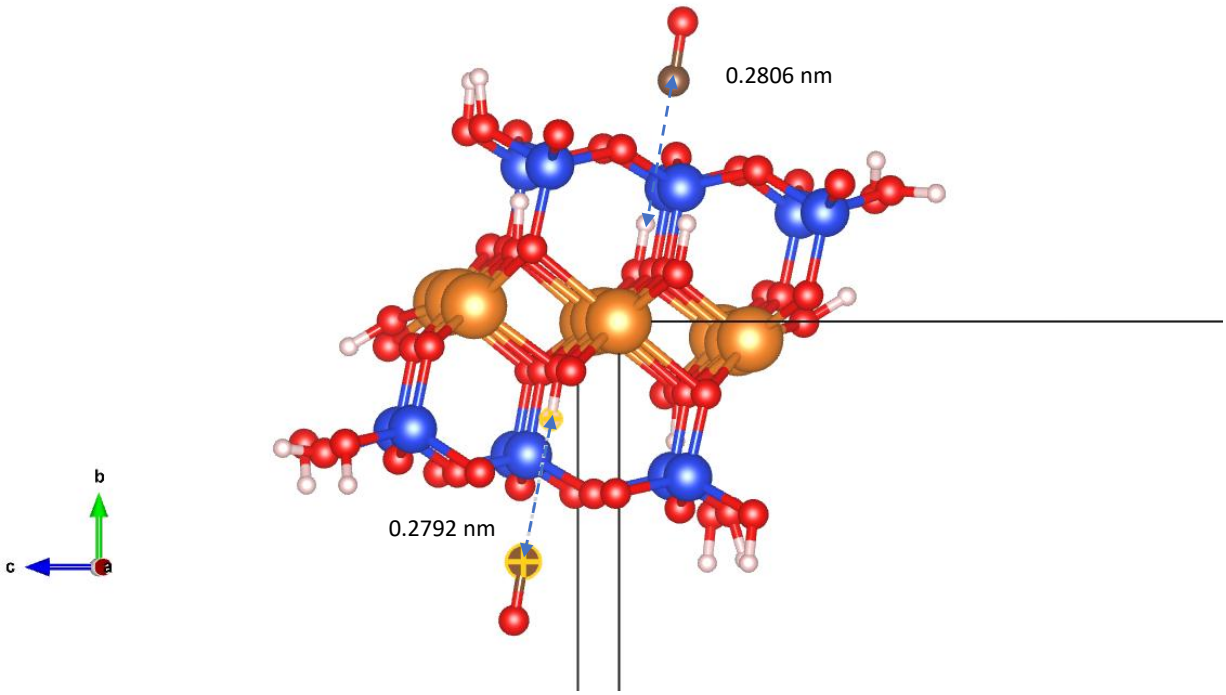

Figure S15 {100} LC_OC_C

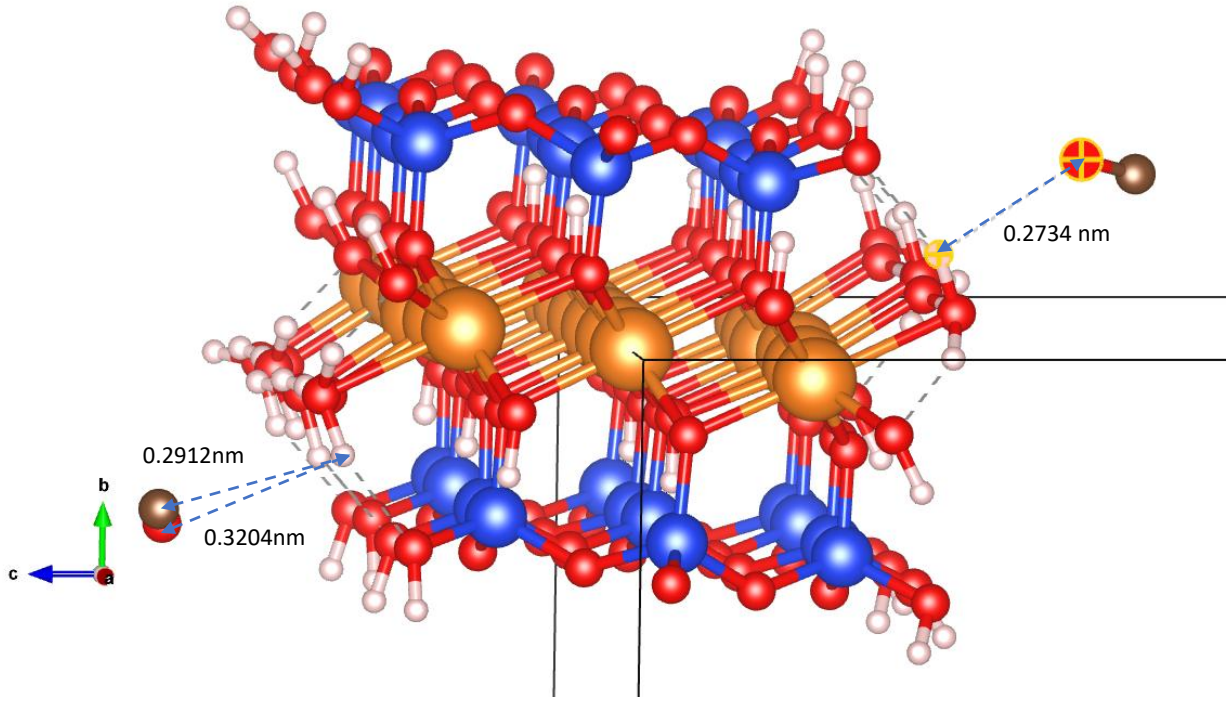

Figure S16 {130} HC_CO_A

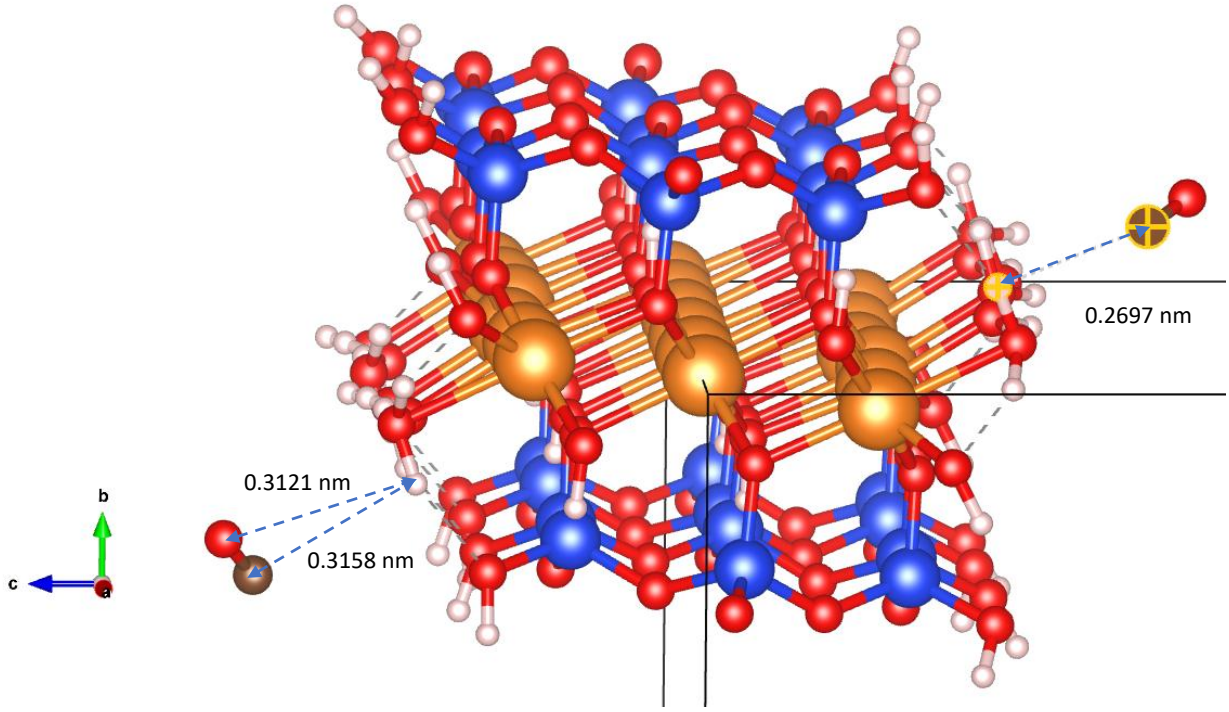

Figure S17 {130} HC_OC_A

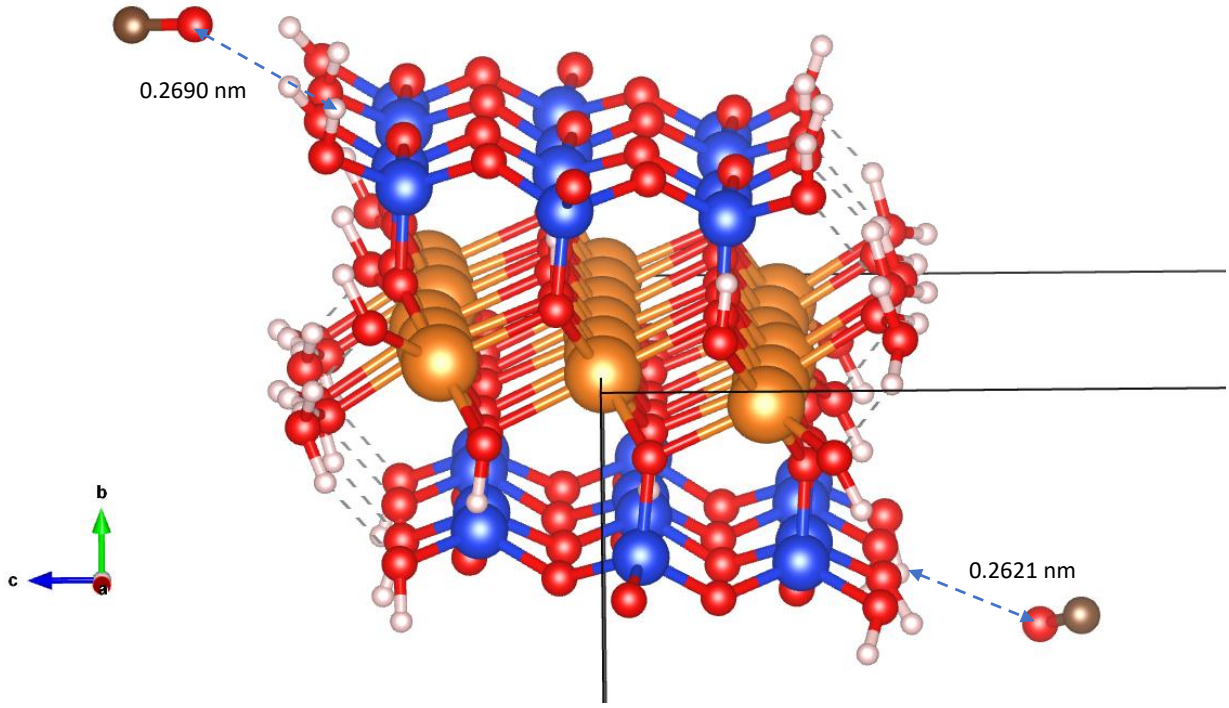

Figure S18 {130} HC_CO_B

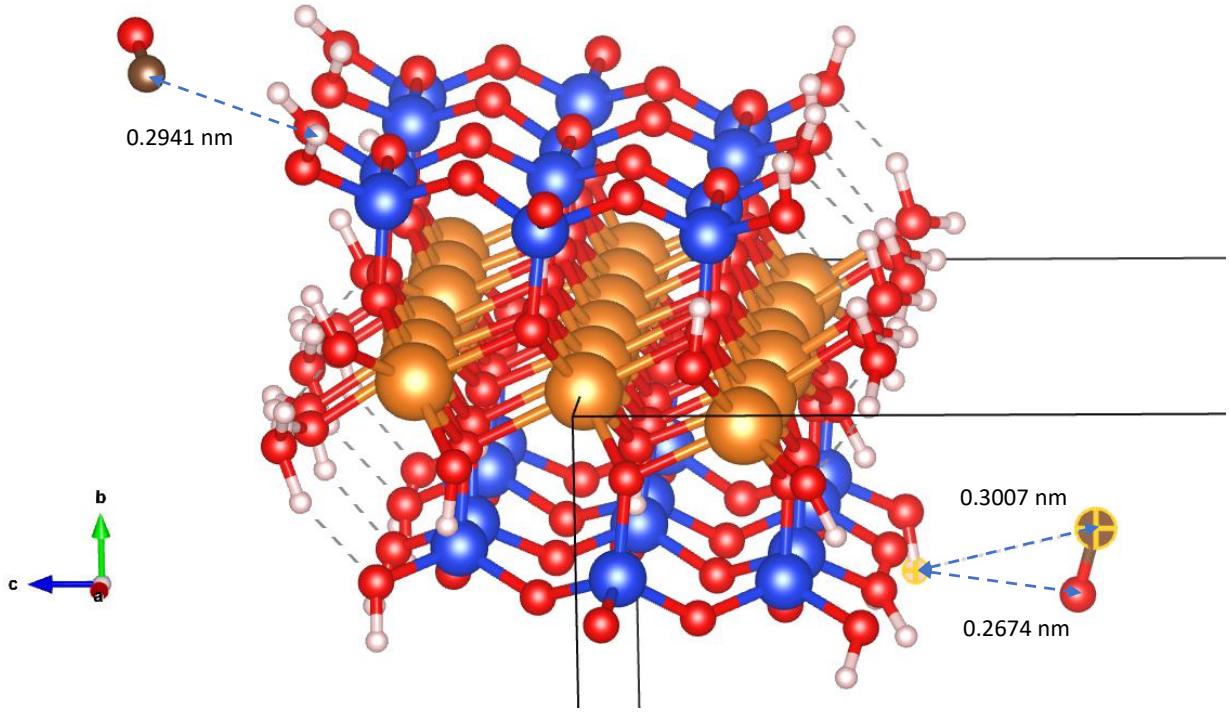

Figure S19 {130} HC_OC_B

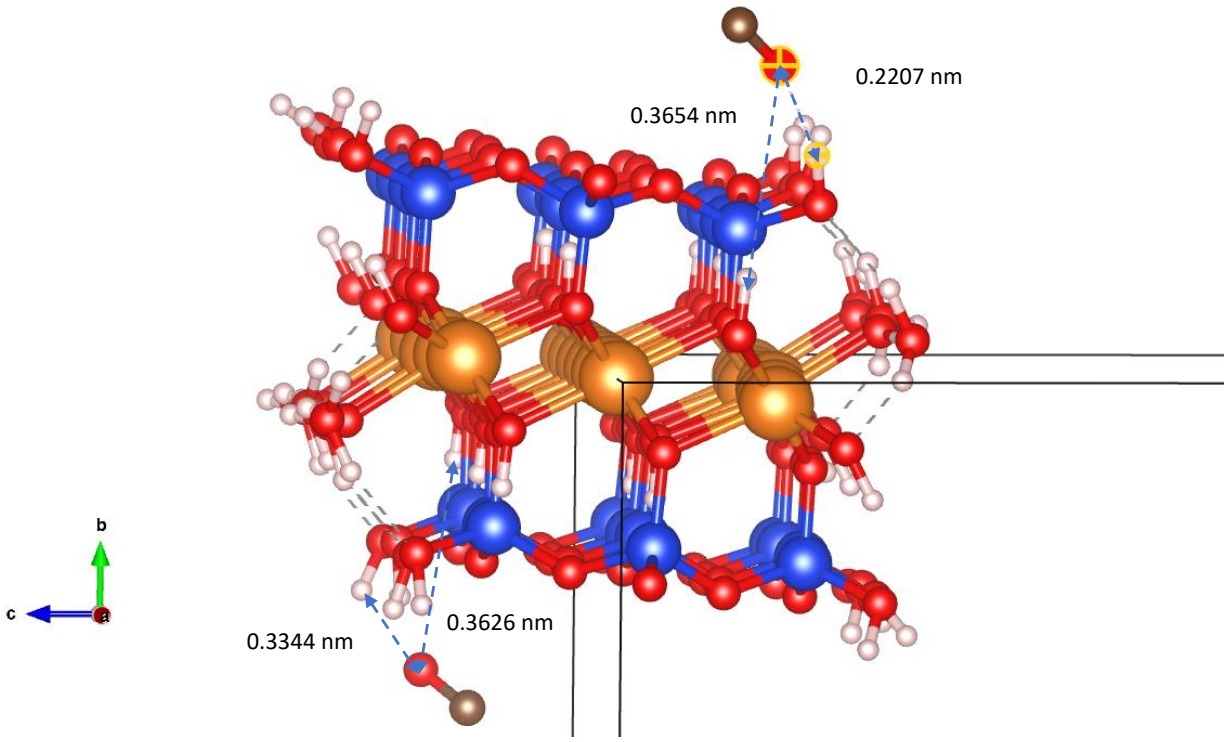

Figure S20 {130} HC_CO_C

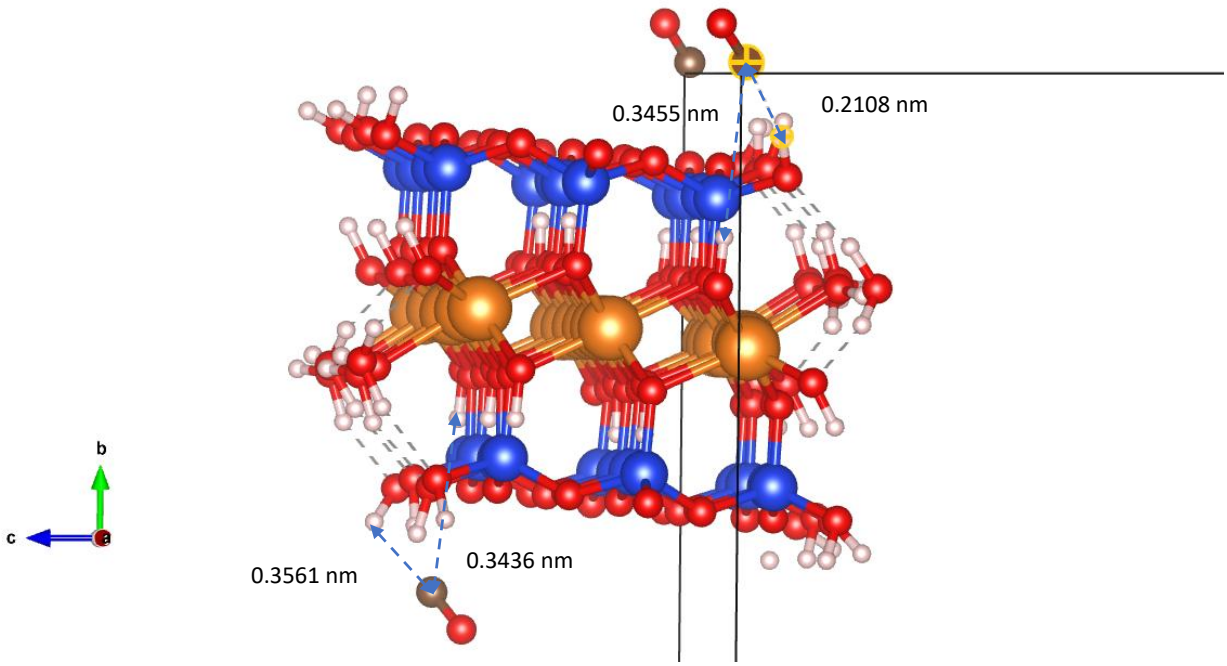

Figure S21 {130} HC_OC_C

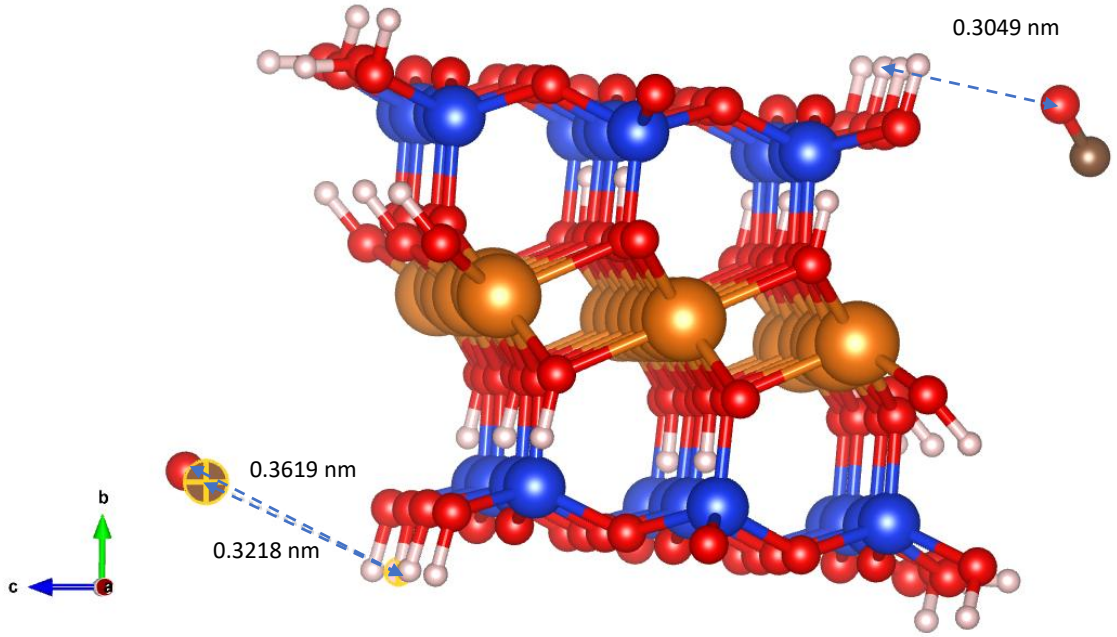

Figure S22 {130} LC_CO_A

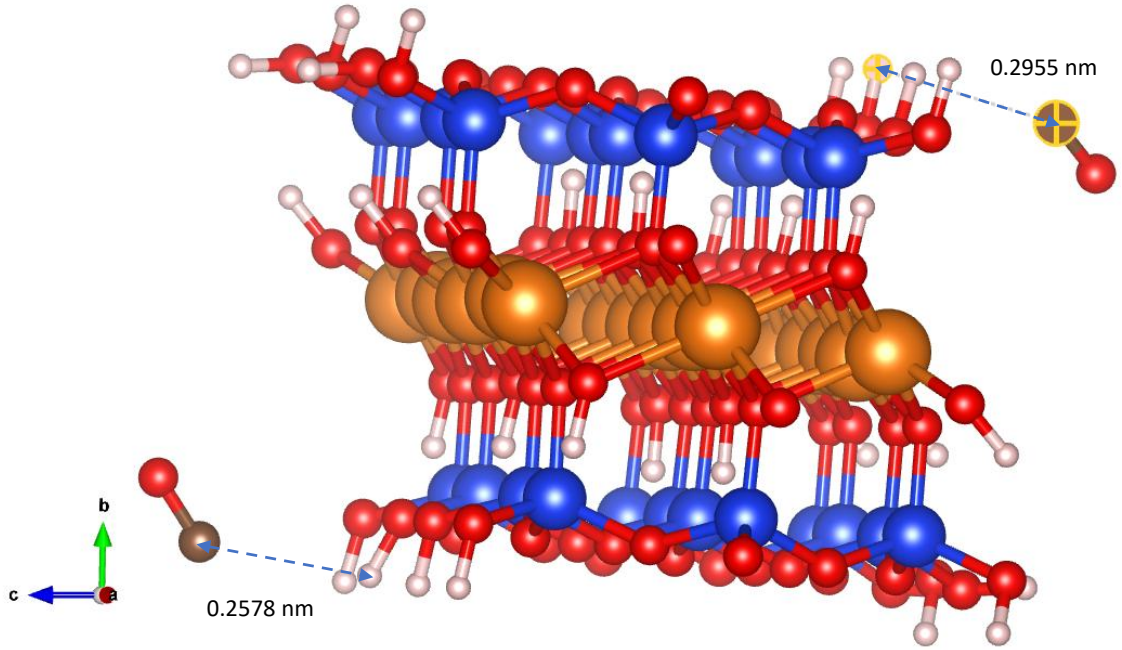

Figure S23 {130} LC_OC_A

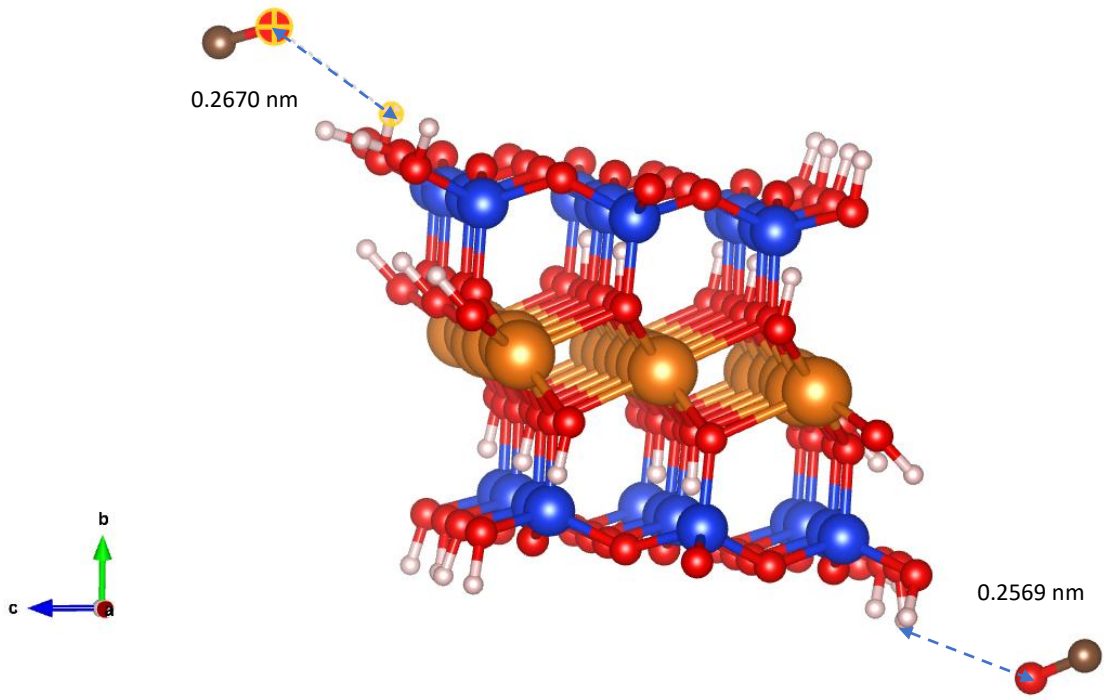

Figure S24 {130} LC_CO_B

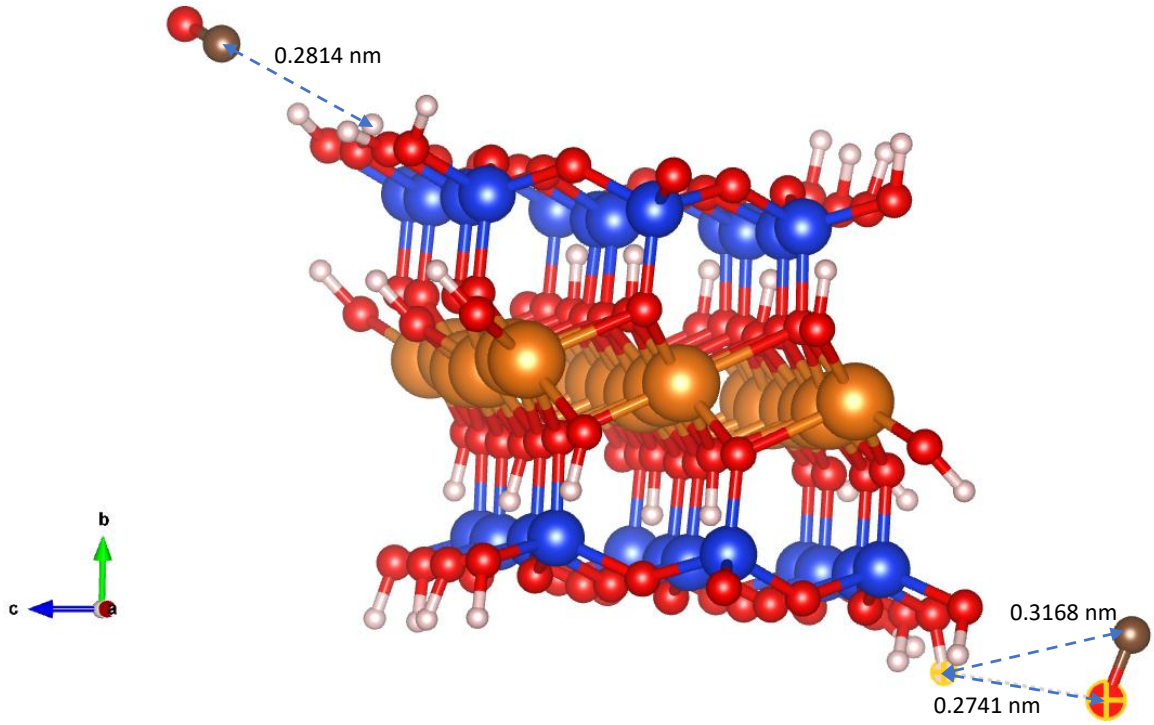

Figure S25 {130} LC_OC_B

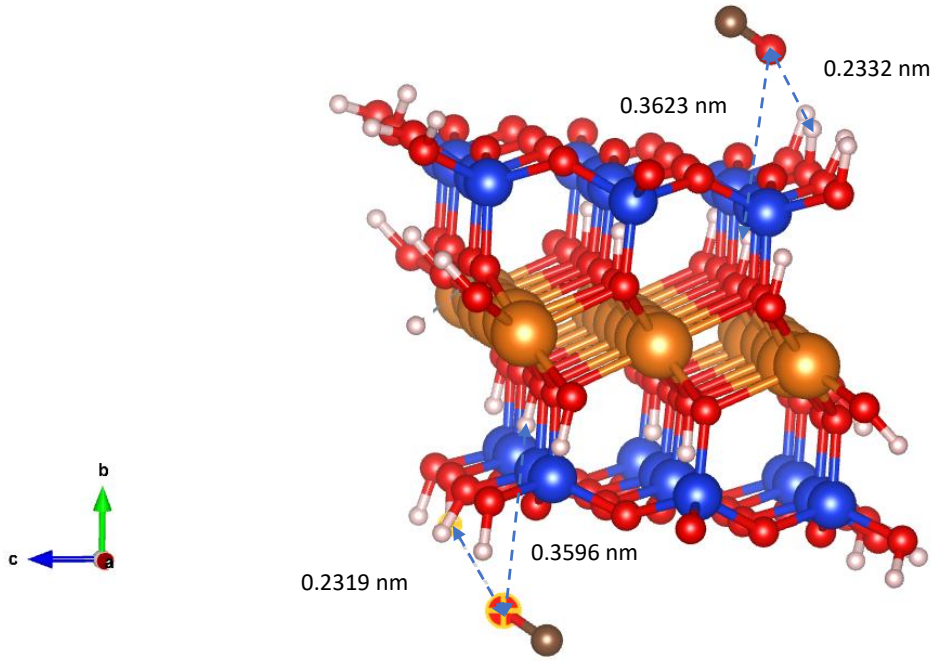

Figure S26 {130} LC_CO_C

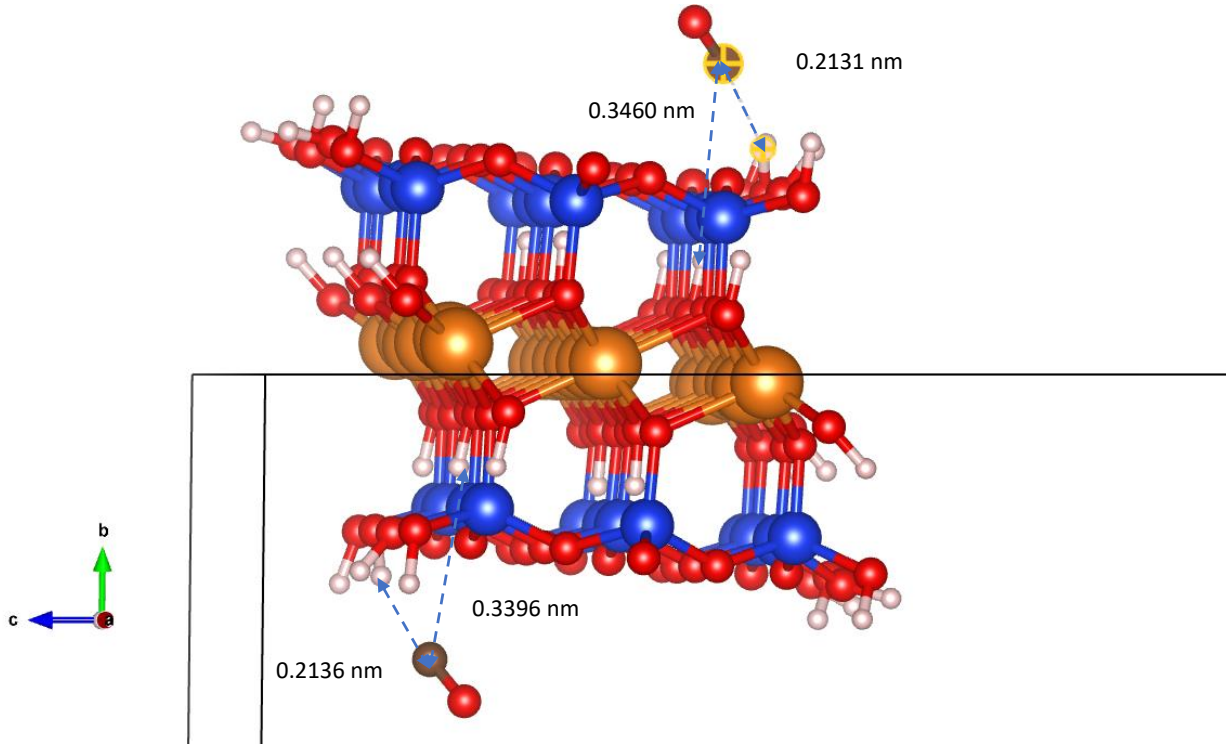

Figure S27 {130} LC_OC_C

4 Experimental transmission FTIR spectra of CO adsorbed on MSH com

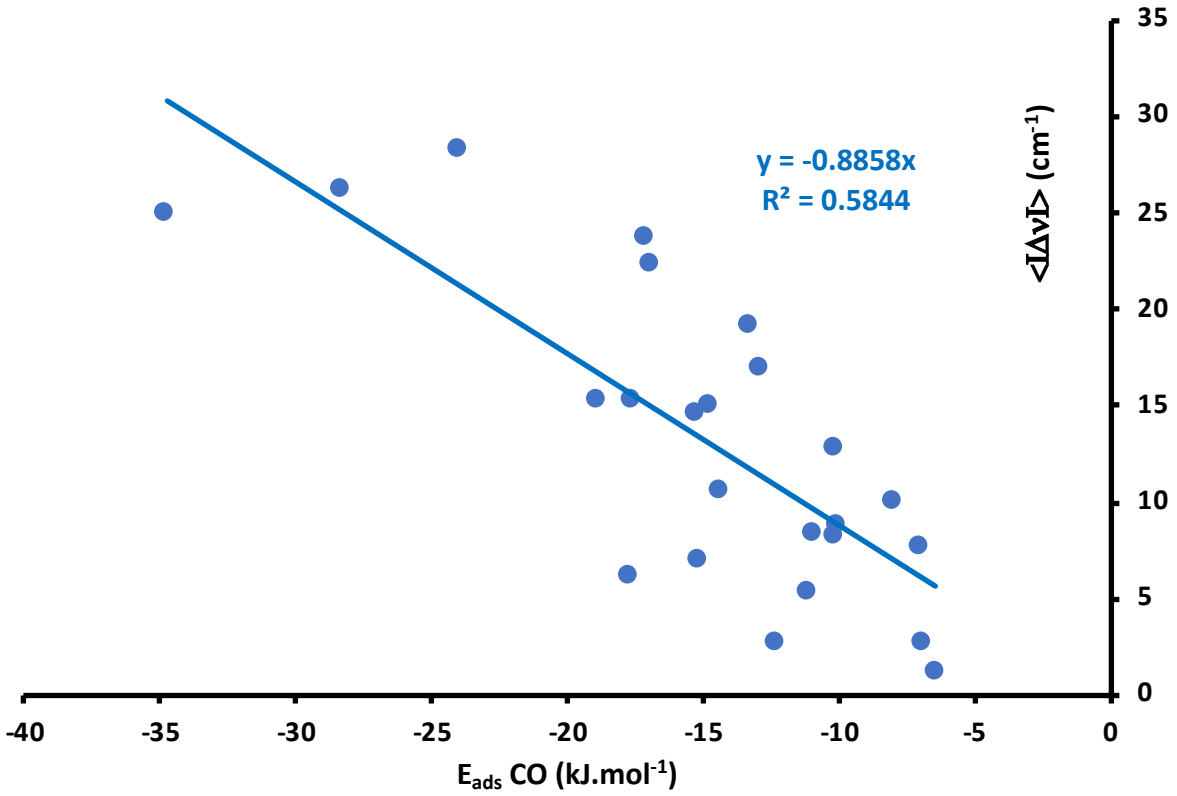

Figure S28: Correlation between average absolute wavenumber shifts and average adsorption energy of CO on HC and LC {100} and {130} A, B and C sites.

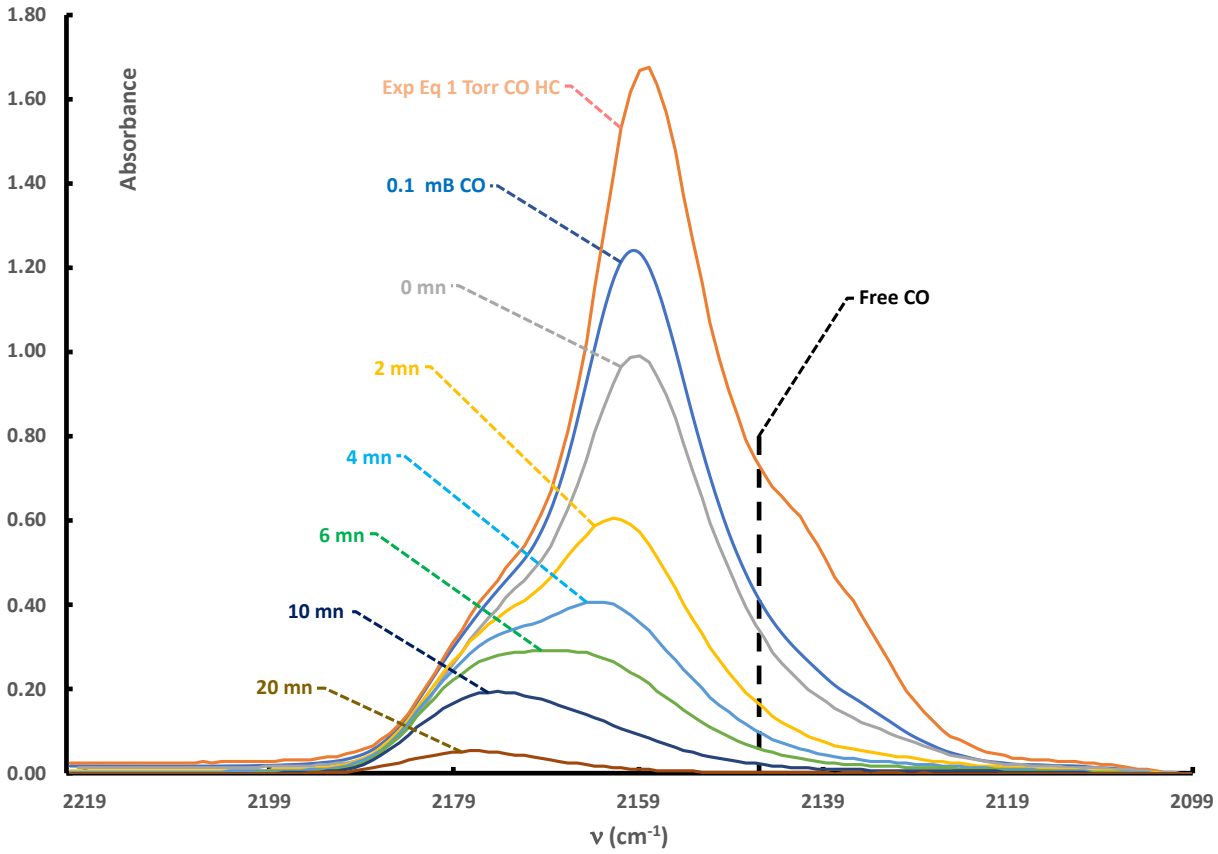

Figure S29: Experimental transmission FTIR spectra of adsorbed CO recorded on MSH com. The sample was pretreated under flowing Argon at 343K, thus predicted to correspond to the high (HC) coverage by water. The spectra (continuous lines) were recorded at 77K: 1) at equilibrium with 1 torr CO (red line); 2) Under static vacuum and 0.1 mB CO (blue); 3) Under dynamic secondary vacuum 0 mn (grey), 2mn (orange), 4 mn (light blue), 6 mn (green), 10 mn (deep blue), 20 mn (brown). The stretching frequency of Free CO is indicated as a dotted black vertical line, in order to separate blue shifted from red shifted parts of the spectra.

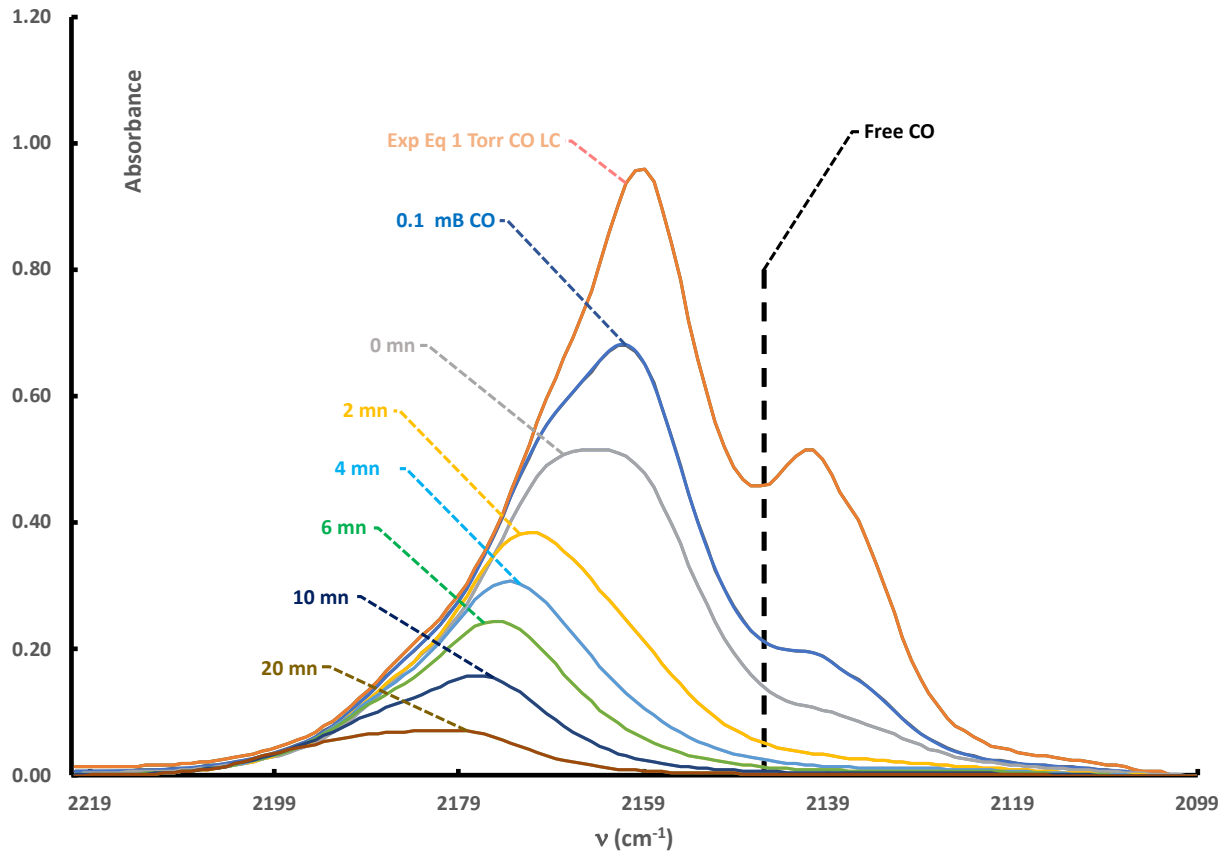

Figure S30: Experimental transmission FTIR spectra of adsorbed CO recorded on MSH com. The sample was pretreated under flowing Argon at 623K, thus predicted to correspond to the low (LC) coverage by water. The spectra (continuous lines) were recorded at 77K: 1) at equilibrium with 1 torr CO (red line); 2) Under static vacuum and 0.1 mB CO (blue); 3) Under dynamic secondary vacuum 0 mn (grey), 2mn (orange), 4 mn (light blue), 6 mn (green), 10 mn (deep blue), 20 mn (brown). The stretching frequency of Free CO is indicated as a dotted black vertical line, in order to separate blue shifted from red shifted parts of the spectra.

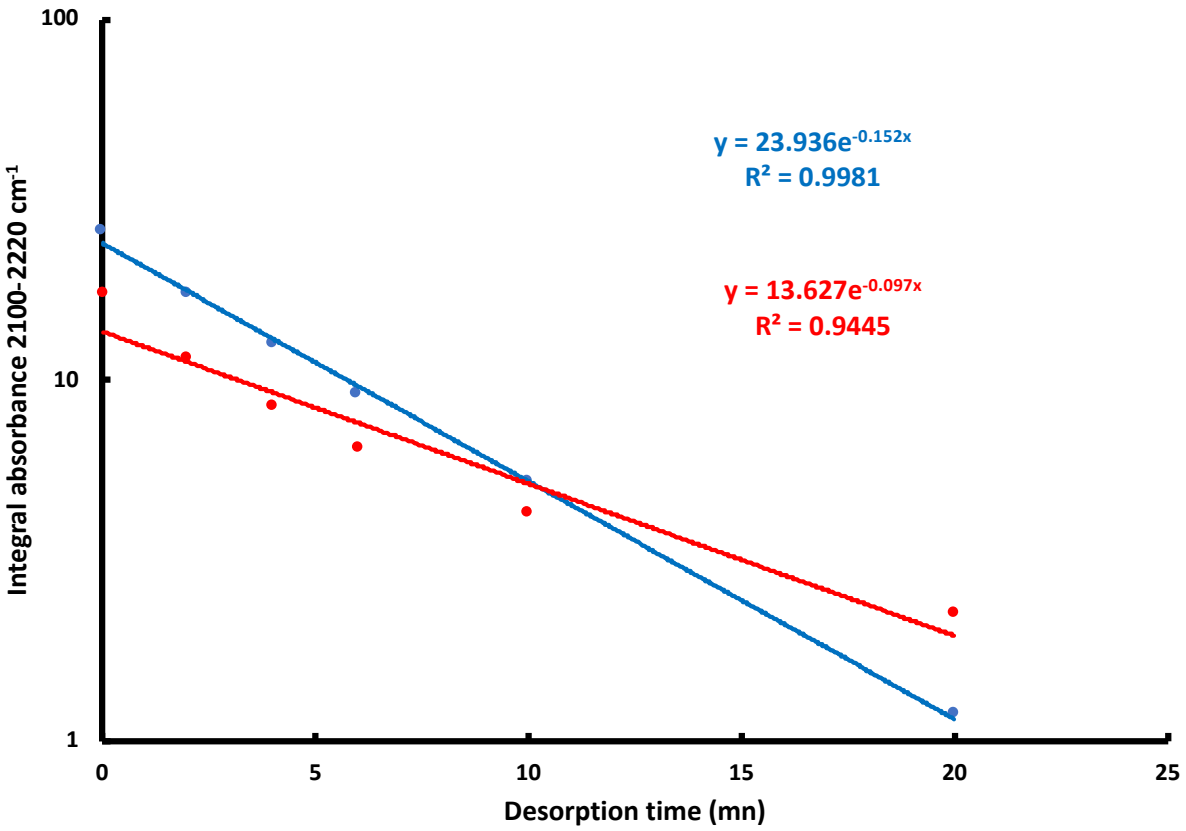

Figure S31: Experimental CO first-order desorption kinetics under dynamic secondary vacuum at 77K, obtained for MSH com pretreated at 343K (HC, blue dots and blue regression line) and 623K (LC, red dots and red regression line). Insets: equations of the regression lines and squared coefficients of correlation.

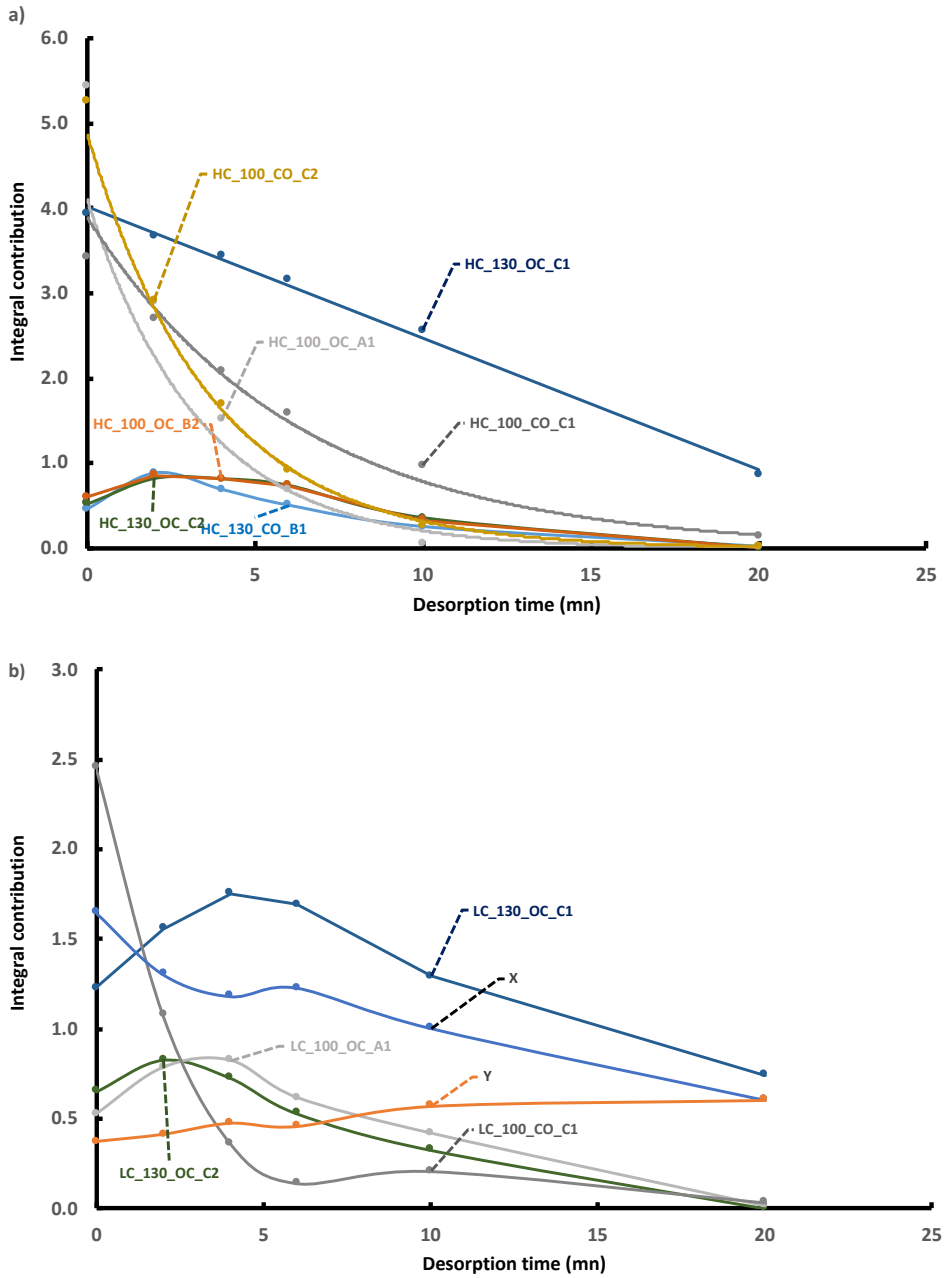

Figure S32: Evolution with desorption time of the main gaussian contributions to simulated CO desorption spectra from a) MSH com pretreated at 343K (HC), average mean absolute deviation of the simulated envelope from the experimental spectrum 0.3 %, average root of variance 6.14 ± 0.04 cm^{-1} ; b) MSH com pretreated at 623K (LC), average mean absolute deviation of the simulated envelope from the experimental spectrum 0.26 %, average root of variance 6.8 ± 0.3 cm^{-1}.

5 Experimental SEM and TEM imaging of MSH com

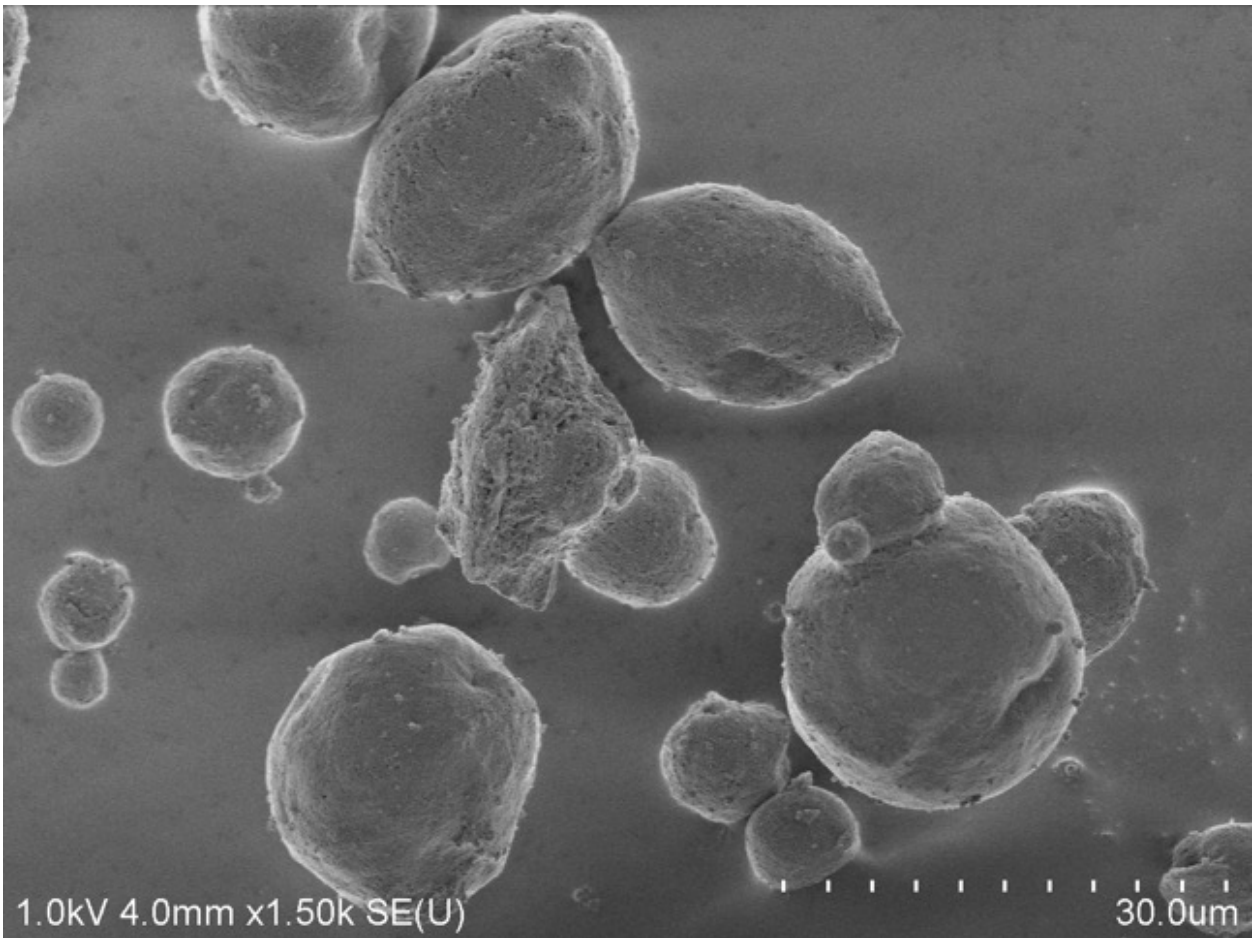

Figure S33: Representative Scanning Electron Microscope (SEM) image of commercial MSH beads (magnification 1500).

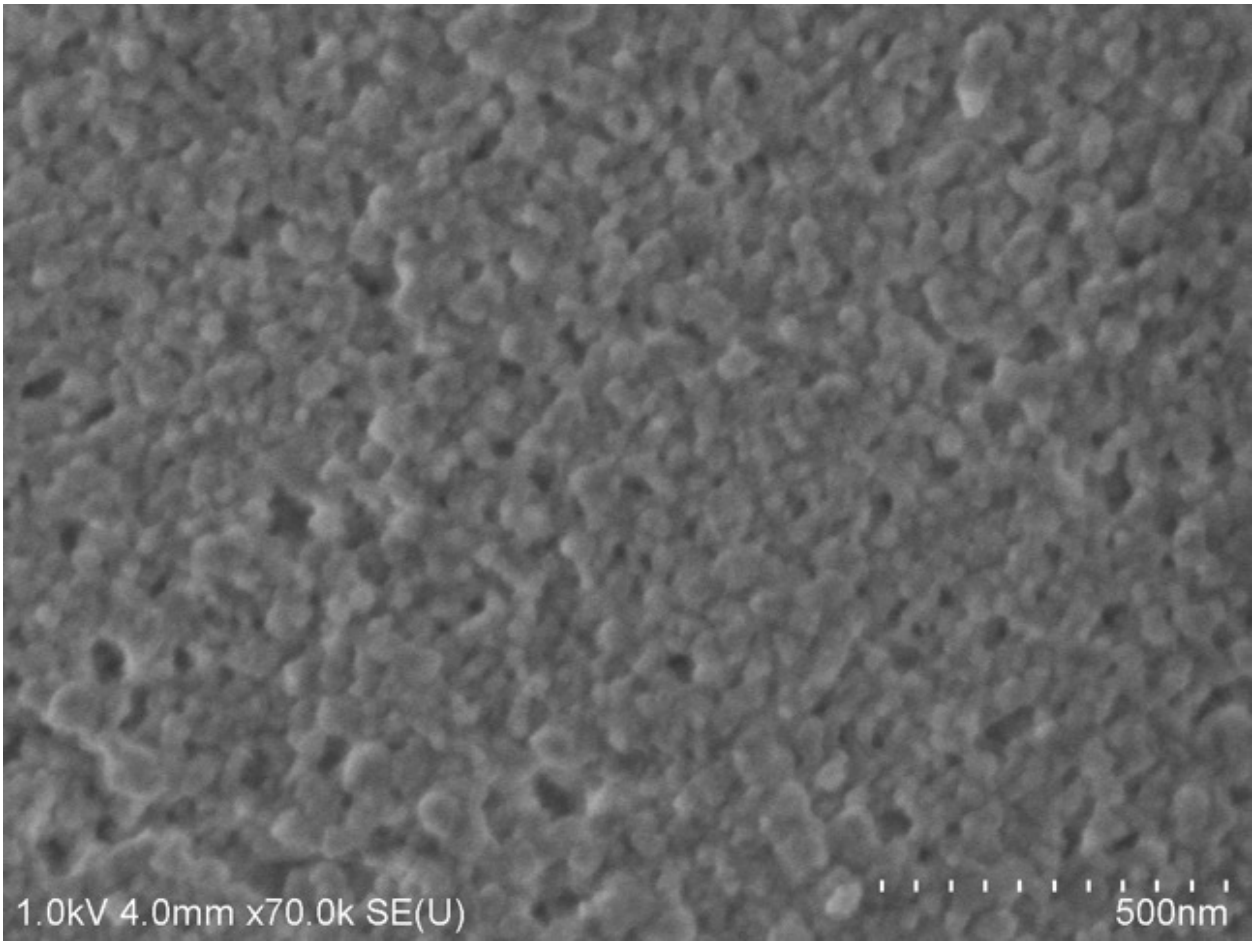

Figure S34: Representative Scanning Electron Microscope (SEM) image of a commercial MSH bead external surface (magnification 70 000).

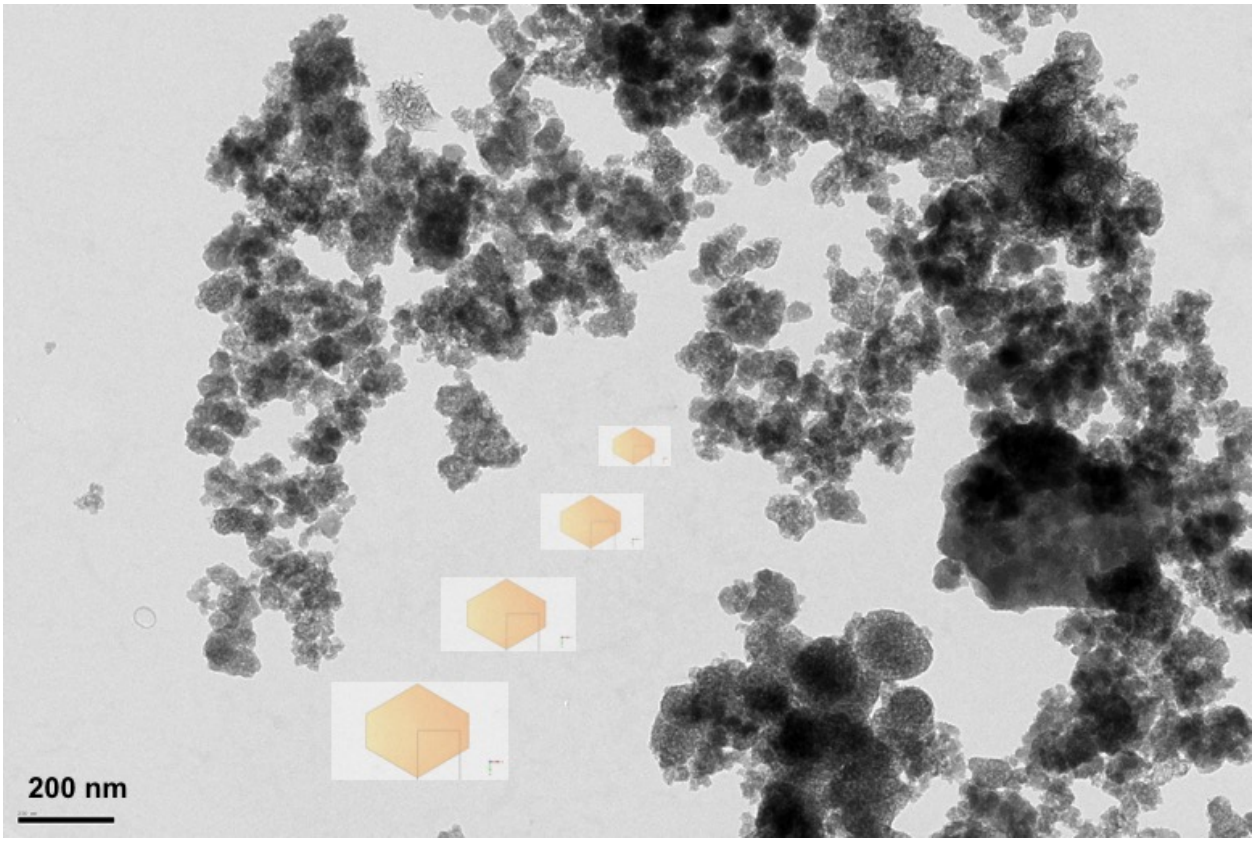

Figure S35: Representative Transmission Electron Microscope (TEM) image of a ground commercial MSH sample (magnification 10 000). Top views of the predicted morphology of nanotalc particles of various sizes are superimposed for qualitative comparison.

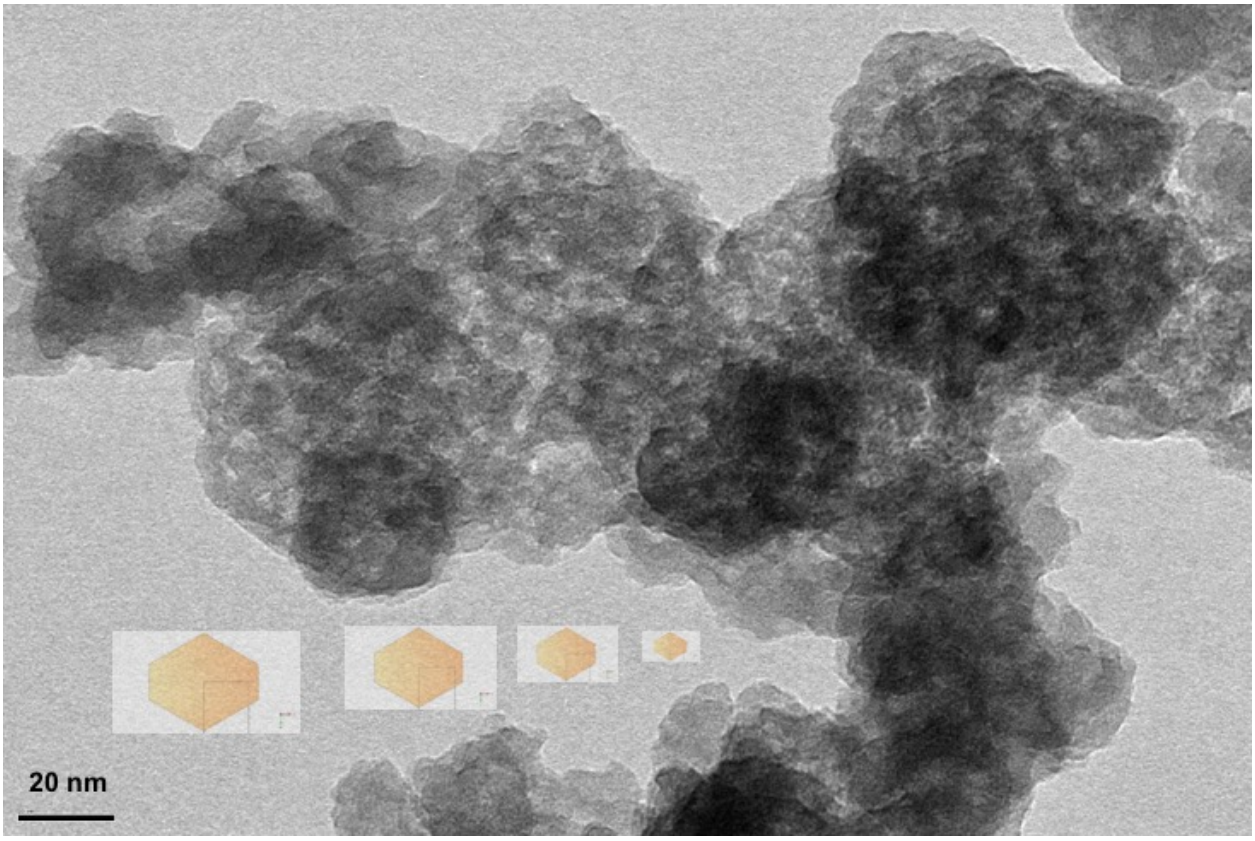

Figure S36: Representative Transmission Electron Microscope (TEM) image of a ground commercial MSH sample (magnification 100 000). Top views of the predicted morphology of nanotalc particles of various sizes are superimposed for qualitative comparison.